Defence Research and Development Canada
Recherche et développement pour la défense Canada

Prediction of Aerosol Hazard Arising from the Opening of an Anthrax Letter in an Open-Office Environment Using Computational Fluid Dynamics

F.-S. Lien and H. Ji
Waterloo CFD Engineering Consulting Inc.
Waterloo, ON

Contract Scientific Authority: E.C. Yee
DRDC Suffield

Contract Report
DRDC Suffield CR 2006-210
October 2006

Canada

Prediction of Aerosol Hazard Arising from the Opening of an Anthrax Letter in an Open-Office Environment Using Computational Fluid Dynamics

F.-S. Lien and H. Ji
Waterloo CFD Engineering Consulting Inc.
534 Paradise Crescent
Waterloo ON N2L 3G1

Contract Number: W7702-05-R099/001/EDM

Contract Scientific Authority: E.C. Yee
DRDC Suffield

Defence R&D Canada – Suffield

Contract Report

DRDC Suffield CR 2006-210

October 2006

Prediction of Aerosol Hazard Arising from the Opening of an Anthrax Letter in an Open-Office Environment Using Computational Fluid Dynamics

Final Report

by
Fue-Sang Lien, Hua Ji
Email: fslien@uwaterloo.ca
Web site: http://www.watcfd.com/

Waterloo CFD Engineering Consulting Inc.
534 Paradise Crescent, Waterloo
Ontario, N2L 3G1

Prepared for
Defence R&D Canada – Suffield

Contract Number: W7702-05R099/001/EDM
Technical Authority: Eugene Yee

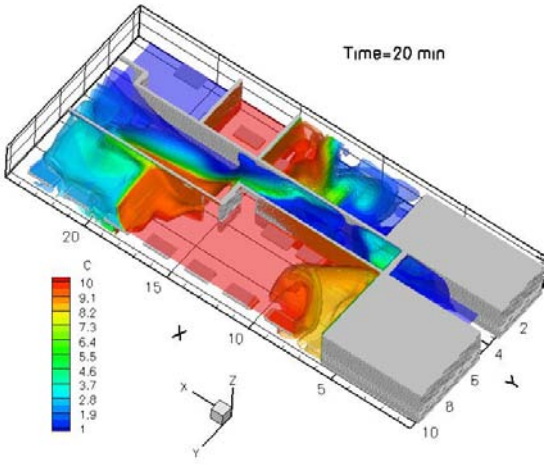

ABSTRACT

Early experimental work, conducted at Defence R&D Canada – Suffield, measured and characterized the personal and environmental contamination associated with simulated anthrax-tainted letters under a number of different scenarios in order to obtain a better understanding of the physical and biological processes for detecting, assessing, and formulating potential mitigation strategies for managing the risks associated with opening an anthrax-tainted letter. These preliminary experimental investigations have been extended in the present study to simulate the contamination from anthrax-tainted letters in an Open-Office environment using Computational Fluid Dynamics (CFD). A quantity of 0.1 g of a biological simulant *Bacillus globigii* (BG) for anthrax was released from an opened letter in the experiment. The accuracy of the model for prediction of the spatial distribution of BG spores in the office from the opened letter is assessed qualitatively (and to the extent possible, quantitatively) by detailed comparison with measured BG concentrations obtained under a number of scenarios, some involving people moving within the office. It is hypothesized that the discrepancy between the numerical predictions and experimental measurements of concentration were mainly caused by

(1) air flow leakage from cracks and crevices in the walls and windows of the building shell;
(2) decoupling between the present CFD simulation and dispersion of BG spores in the Heating, Ventilation, and Air Conditioning (HVAC) system;
(3) the effect of deposition and re-suspension of BG spores not being considered in the present CFD simulations.

Although there is still a scope of further improvement in the present CFD simulation, it should be emphasized here that the advantages of utilization of CFD modeling for assessment and design of mitigation strategies and protocols for defence against anthrax-tainted letters over an experimentally-based approach to the problem are obvious:

(1) substantial reduction of lead times and costs of new designs involving other office configurations;
(2) ability to study scenarios where controlled experiments are difficult or impossible to perform;
(3) practically unlimited level of detail of results such as the flow field in the indoor environment and the concentration field of the dispersing BG spores (or, other contaminants) that are released into this flow field.

Table of Contents

List of Figures

1. INTRODUCTION

The incident involving anthrax-tainted letters sent in the autumn of 2001 to major media outlets and two United States senators that resulted in five deaths and 17 non-fatal infections has reinforced public concern on the threat of terrorist use of chemical and biological warfare (CBW) agent weapons against civilian populations in dense urban centers. In some previous experimental work, Defence R&D Canada – Suffield has measured and characterized the personal and environmental contamination associated with simulated anthrax-tainted letters under a number of different scenarios in order to obtain a better understanding of the physical and biological processes for detecting, assessing, and formulating potential mitigation strategies for managing the risks associated with opening an anthrax-tainted letter. These preliminary experimental investigations have been extended recently to characterize the contamination from anthrax-tainted letters in an Open-Office environment.

Practical mathematical models for prediction of dispersion of anthrax spores from opened letters in an indoor environment, including people moving within various offices, do not exist owing to the inherent complexity of the problem. There are an enormous number of possible scenarios for incidents involving anthrax-tainted letters due to their deliberate nature. Furthermore, the physical insight and concomitant data necessary to perform and validate the model predictions for most scenarios involving anthrax-tainted letters are (until recently) limited. In addition, the parameters required by the model (e.g., deposition velocity of anthrax spores with respect to various surfaces) and the data needed to infer these parameters may not be available. In spite of these complications, it should be emphasized that computational fluid dynamics (CFD) is a field that is advancing by leaps and bounds and it will be demonstrated by the present study that CFD is able to predict credibly both flow characteristics inside buildings (and, more specifically in an office within a building) and the dispersion of contaminants (e.g., anthrax spores from an opened letter) released into these flows.

The objective of the present study is to undertake a critical assessment of the utility of current state-of-the-science CFD models for the prediction of flow and dispersion in the indoor environment. In particular, CFD modeling of the dispersion of a biological simulant *Bacillus globigii* (BG) for anthrax released from an opened letter in a large office (Open-Office concept) will the undertaken, and the accuracy of the model for prediction of the spatial distribution of BG spores in the office will be assessed qualitatively (and to the extent possible, quantitatively) by detailed comparison with measured BG concentrations obtained under a number of scenarios. In Sec. 2, the basic numerical framework for the CFD model used for these numerical studies, including a new capability for simulating people moving within various offices will be described. Sec. 3 will compare predictions against a baseline experiment whereby a tracer gas sulfur hexafluoride (SF_6) was released in an open office in the west wing of Building 13 at DRDC-Suffield. In Sec. 4, three scenarios involving the release of BG spores from an opened letter will be described, and various comparisons between model predictions and

experimental measurements will be made for each scenario. Finally, conclusions drawn from the present study and recommendations made for future studies are given in Sec. 5.

2. NUMERICAL METHOD

The STREAM code [1], used in the present study, is a fully-conservative, block-structured finite-volume program for computational fluid dynamics, which employs a fully-collocated storage arrangement for all transported properties, including all turbulence quantities (turbulence kinetic energy, viscous dissipation rate, etc.). Within an arbitrary non-orthogonal coordinate system, the velocity vector is decomposed into its Cartesian components, and these are the components to which the momentum equations relate. Advective cell-face fluxes are approximated by the Upstream Monotonic Interpolation for Scalar Transport (UMIST) scheme [2], obtained by formally imposing Total Variation Diminishing (TVD) constraints on Leonard's third-order accurate Quadratic Upstream Interpolation for Convective Kinematics (QUICK) scheme [3]. A second-order fully implicit three-level scheme is used to treat the transient (or, local tendency) term. The mass continuity is enforced by solving a pressure-correction equation using the Semi-Implicit Method for Pressure-Linked Equations (SIMPLE) algorithm, which steers, as part of the iterative sequence, the pressure towards a state in which mass residuals in all cells in the flow domain are negligibly small. All transport equations, including momentum, turbulence and scalar concentration equations, are discretized and solved sequentially as part of the SIMPLE algorithm [4] using very efficient iterative linear equation solvers such Stone's Strongly Implicit Procedure (SIP3D) or the Conjugate Gradient Stabilized (CGSTAB) method. In conjunction with a fully-collocated approach, the SIMPLE method is known to provoke checkerboard oscillations in the pressure field, reflecting a state of velocity-pressure decoupling. To avoid this, the widely used method of Rhie and Chow [5] has been adopted to interpolate the cell-face velocities from adjacent nodal values. The interpolation essentially introduces a fourth-order "pressure smoothing" to remove the checkerboard oscillation in the pressure field. Physical diffusion fluxes are approximated using a conventional second-order accurate central differencing approach.

For mesh generation, the "ray-casting" approach [6] is used to determine whether the computational cells are inside the complex geometries encountered in the current problem, such as desks and bookcases in the study area. If the cell centroid is inside an obstacle, the associated cell flag will be set to OBSTACLE. Otherwise, the cell flag will be set to FLUID so that an efficient matrix solver, such as SIP3D can be utilized.

In order to numerically model one or more persons "entering or leaving" the office, the Immersed Boundary Method (IBM) [7] or its variants [8] were used to handle moving objects. The original IBM [7] represents the body boundary in the flow field through a forcing term (or a feedback function) that is added to the momentum equations. These forcing terms are evaluated initially at the discrete surface points, and satisfy the no-slip boundary conditions on the surface. Subsequently, a first-order cosine function, which can be interpreted as a discrete function, is used to interpolate and extrapolate

information between the immersed boundary and the background grid. Unfortunately, the use of the cosine-function formulation smears out the solutions over a thin finite band centered on the boundary, which in general could have an adverse effect on the solution accuracy. Furthermore, IBM may induce spurious oscillations and consequently restrict the computational time step, especially when an explicit time-integration method is used for the flow solver.

To overcome this difficulty, other IBM variants, such as the ghost-cell immersed boundary method (GCIBM) [8] have been proposed. In contrast to IBM, GCIBM uses ghost cells within the solid objects as boundary conditions without having to explicitly introduce a forcing term into the momentum equation. The ghost cells are reconstructed using either linear or quadratic interpolation of property values at the surrounding fluid nodes in the physical domain and at a boundary node. Although IBM has been widely used, most previous researchers have incorporated it into *explicit* flow solvers based on a fractional-step method which severely limits the maximum allowable time step that could be used for the integration. Moreover, very little work has been undertaken to date in combining IBM with high-Reynolds-number Reynolds-averaged Navier-Stokes (RANS) solvers for turbulent flow problems. In the present study, we have successfully incorporated the GCIBM into STREAM to give a fully implicit time-stepping scheme that utilizes a standard k-ε turbulence model in conjunction with wall functions as boundary conditions at the solid surfaces (e.g., walls). This is an innovation developed in the present study for the simulation of moving objects (e.g., people) within the flow domain.

3. SULFUR HEXAFLUORIDE (SF_6) RELEASE EXPERIMENTS

The SF_6 experiment [9] was conducted by personnel from National Institute for Occupational Safety and Health (NIOSH) in the USA on September 12-19, 2005. The flow rates in cubic feet per minute (CFM) for the supply and return ducts in the study area (see Fig. 1) in Building 13, which is located on Canadian Forces Base Suffield, were measured. This information will be used as the inflow/outflow boundary conditions for the present CFD simulations. Five tracer gas studies were conducted, and only data from "Experiment 1" will be used for comparison with CFD predictions. In this experiment, 2.5 liters of pure SF_6 was delivered by an airtight syringe at Location F (letter-opener position) in Fig. 1. Measurements of the time history of the SF_6 concentration in parts per million (ppm) are available at 7 locations (Locations A-G) as shown in Fig. 1.

Since dispersion of SF_6 in the study area is strongly influenced by the flow motion, it is informative to examine the model predictions of the flow field first, which are obtained for the study area (Open Office) with a grid of 94×70×30 nodes in the *x*-, *y*- and *z*-directions, respectively. This grid used here is exhibited in Fig. 2. Initially, it is assumed that the direction of airflow from the air supply ducts is in the vertical (or *z*-) direction as indicated by the "big" arrows in Fig. 3. To understand the flow field in the study area, let us consider a vertical *y*-*z* cross-section in Area I near Location F as illustrated by a sketch on the right-hand-side of Fig. 3. We expect to see a clock-wise vortex motion when a jet is discharging from the bottom-left corner, representing one of the air supply ducts

mounted on the floor. The implication of this figure is that the flow motion in the selected *y*-*z* plane can be quite energetic, but the flow motion in the *x*-direction is actually quite weak as is clearly shown in Fig. 4 in terms of stream traces near the front part of the study area. Bear in mind that the average velocity from the supply and return ducts is about 1 m s^{-1}. The magnitude of the average velocity in the study area is about 5 cm s^{-1}. The average velocity in the *x*-direction is around -0.2 cm s^{-1}, which confirms the above-mentioned assertion of weak flow motion in the *x*-direction. The stream traces in the entire study area are exhibited in Fig. 5, which will be used to facilitate our discussion of the SF_6 dispersion results to be shown later.

The release period for the SF_6 tracer is assumed to be T_{ON} = 10 sec in the CFD simulation, although a release period of 5 sec was also attempted with little effect on the final solution. In order to increase the time accuracy of the numerical prediction, the time step, Δt, for the simulation was chosen based on the following table:

Δt = 0.2 sec	Δt = 2 sec	Δt = 10 sec
$t \le T_{ON}$	$T_{ON} < t < 2$ min	$t \ge 2$ min

The total time for the simulation is 2 hours after the initial release of the SF_6 tracer. The predicted time histories of the mean concentration SF_6 at Locations A, B, C, D, E, and G and their comparison with the corresponding experimental measurements are shown in Fig. 6. At Location A (collocated with co-worker 1), there is a sharp increase in the concentration-time profile in the experimental measurement, reaching a peak value of 20 ppm at t = 3 min (i.e., at 3 min after the SF_6 tracer was released). This peak concentration occurs much earlier than that predicted by the numerical simulation at the same location, where the predicted peak value of concentration is seen to be 10 ppm occurring at t = 13 min. Similarly, at t = 5 min, the experimental concentration measurements at Location B (where co-worker 2 is located) achieves a peak concentration value of 11 ppm, which is again larger than the predicted concentration value of 6 ppm and occurs also at a much later time of t = 50 min. In order to identify what might be the cause of the discrepancy in the predicted and observed cloud arrival times, two additional simulations were conducted. Firstly, a simulation was conducted for the same test problem using a finer mesh of 140×100×70 nodes. However, this higher-resolution simulation gave essentially the same results as the original simulation. Since air flows through the supply ducts are deflected by grilles, for the second additional simulation the direction of air flow at each supply duct location was deflected by ±45° as illustrated in Fig. 7. Again, no major changes were observed in the predicted results. A number of reasons could be the cause of the above-mentioned discrepancy between the predicted and observed SF_6 concentration-time histories. These are as follows:

1. In the real situation, SF_6 released from Location F can enter the return ducts (there are two return ducts in Area I) and, through the HVAC system re-enter the study area again through the supply ducts. However, this physical mechanism is not considered in the present CFD simulation. Although there are some ‘zonal models’, such as COMIS [10] and CONTAM [11], which are designed specifically for predicting dispersion of contaminant in the indoor environment, including the HVAC system,

these models are one-dimensional (1-D) and cannot be applied to the simulation of the complex 3-D flow and dispersion in a large office with furniture. The remedy for this problem is to develop a general procedure, which can couple the present CFD model (used to simulate the 3-D indoor flow and dispersion in the study area) with one of the zonal models (which can be used to simulate the 1-D flow and dispersion in the HVAC system).

2. Building 13 at DRDC-Suffield is a very old building that was built during the Second World War. It is very likely that the draft from leakage in windows and walls generate additional flow motion in the office, which can enhance the dispersion of the SF_6 tracer at Locations A and B. A "blower door"[1] experiment might be required to identify the locations of the leakage points and flow rates through these points in the shell of Building 13. Certainly, with this additional information, it is anticipated that the predictive accuracy of the current CFD simulation results can be improved.

In addition to the two reasons enunciated above, experimental anomaly can also be a contributing factor to the discrepancy between the CFD predictions and the experimental measurements. To see this, let us also examine the results of Experiment 5 from [9] as shown in Fig. 8. The major differences between Experiments 1 and 5 are given below:

	Tracer	Release mechanism	Release period
Experiment 1	Pure SF_6	An air-tight syringe	30 sec
Experiment 5	Dilute SF_6	A sampling pump	1 min

Note that in Experiment 5, one liter of pure SF_6 was combined with 3 liters of outdoor air. However, the relative ratio of peak concentrations at Locations A, B and D for both experiments should be very similar. It is seen from Figs. 6 and 8 that $(C_A:C_B:C_D)_{peak}\approx(6.75:3.7:1)$ for Experiment 1 and $(C_A:C_B:C_D)_{peak}\approx(22.7:1.1:1)$ for Experiment 5, where 'C' denotes the concentration and the subscript on C indicates the location where the concentration was measured. In the present simulation, $(C_A:C_B:C_D)_{peak}\approx(1.75:1:1)$. If we simply look at $(C_B/C_D)_{peak}$, we find that $(C_B/C_D)_{peak} \approx 1.1$ from Experiment 5 is very close to the present prediction of $(C_B/C_D)_{peak} \approx 1$, which is very encouraging. This seems to suggest that the much larger value of C_B (concentration at co-worker 2 location) measured in Experiment 1 may be questionable. It should be mentioned here that the very large peak value of concentration at Location A (where co-worker 1 is located) relative to the concentrations at the other sampler locations in Experiment 5 is probably also suspect. This assertion will be supported in Fig. 22 for Scenario 0 in the BG experiment (to be discussed later).

With reference to Fig. 6, the "well-mixed" condition, for which concentration levels at all sampler locations are very similar, is clearly shown to be achieved (approximately or better) when $t \geq 50$ min in Experiment 1. However, even after 2 hours, the well-mixed condition was not achieved in our numerical simulation, particularly at Locations A (co-

[1] A blower door is a large calibrated fan that is temporarily mounted in a house door to measure the "leakiness" of the house and to assist in finding the location of the leaks (http://www.infiltec.com/inf-bd.htm).

worker 1) and E (sampler in Area IV), which is consistent with the iso-surfaces of concentration in ppm at t = 3, 20, 60 and 120 min (after the release) shown in Figs. 9 to 12.

Finally, in order to demonstrate the capability of our CFD simulations in predicting accurately a transient release of tracer in a 'well-controlled' laboratory experiment, sample results from [12] in terms of the time history of a mean concentration profile along the vertical center plane of the obstacle array (y = 0) and z/H=0.25 (H is the height of the obstacles) is given in Fig. 13. As can be seen, excellent agreement between predictions and measurement was achieved. Although agreement between the present CFD simulations and measurements for Experiment 1 is less satisfactory, a result that is probably due to air flow leakage through the shell of Building 13 among other things, recommendations for further improvement of the present predictive results will be made in Sec. 5.

4. BACILLUS GLOBIGII (BG) RELEASE EXPERIMENTS

These experiments were conducted by technicians from Dycor Technologies Ltd., in which several scenarios involving the release of BG spores from an opened letter were studied. Only 3 scenarios described in Sec. 4.1 to 4.3 were simulated by CFD.

4.1 Scenario 0 (Baseline Case):

A source of 0.1 g BG spores was placed in a sealed envelope which was located at the location of "Letter Opener" (LO) shown in Fig. 14. To simplify the notation henceforth, Co-worker 1 and Co-worker 2 in Fig. 14 will be denoted by CW1 and CW2, respectively. The LO (person) was located in front of the source location (sealed envelope) by about 50 cm. The office geometry and grid, containing 116×74×30 nodes in the x-, y- and z-directions respectively, is shown in Fig. 15. Note that the major differences between Figs. 2 and 15 are that partitions were added in-between the various desks in the study area and the two middle doors in Area I (Fig. 15) were closed. The HVAC system was turned on for about 15 min until the flow reaches a pseudo-steady state condition before the sampling process began, the latter lasting for another 30 min. During the sampling stage, the HVAC was still on, and the front and rear doors in Area I were open. Similar to the SF_6 experiment described earlier, BG spores entering the return ducts are assumed to be discharged directly to the outdoor environment (viz., no spores entering the return ducts were allowed to re-enter the study area through the supply ducts) in the present simulations. The (unknown) effects of deposition and re-suspension of BG spores in the study area were not considered here (viz., walls and other surfaces in the Open Office are assumed to be *perfect reflectors* in the sense that no BG spores are assumed to be deposited on these surfaces). Immediately after the BG spores were released (viz., the letter was opened), the LO remained stationary for the remainder of the test period. The total release period for the BG spores was assumed to be 10 sec.

Contours of log[100C], where C is the concentration in g m^{-3}, are shown in Fig. 16 at t = 8.75 sec and in Fig. 17 at t = 30 min. Note that in contrast to Figs. 26 and 31 for Scenario 1 (to be shown later), the presence of the LO in Fig. 16 obstructs the spread of BG spores (viz., the extent of contours of concentration in Fig. 16 is much less than those in Figs. 26 and 31, in which the LO moves through the study area and has already left Area I). Concentration contours in Fig. 17 suggest that BG spores have already dispersed into the entire study area at t = 30 min, with concentrations in regions close to Area IV (the green region) being the smallest.

In the present study, the unit for concentration "C" shown in Figs. 18, 19, 21 and 23 is g m^{-3}, which is different from ACPLA (Agent Containing Particles Per Liter of Air used in the measurements made by the slit samplers) in Figs. 22 and 24 and [CFU (Colony Forming Unit) per Liter of Air used by the SKC samplers] in Fig. 20. Since the exact conversion between g m^{-3}, ACPLA and CFU per Liter of Air is unknown, each comparison between the present CFD results and the experimental data needs to be interpreted with care. In performing the analysis of the filters from the SKC samplers in the experiment, the data from the slit samplers were used to determine the cloud arrival time at each location. Here the cloud arrival time at each location is estimated in accordance with its time history at each SKC location. For example, by reference to Fig. 18, T_{start} = 273 sec at SKC-2. This is used as the start time to compute the time-averaged concentration using the following formula:

$$\overline{C} = \frac{1}{T_{end} - T_{start}} \int_{T_{start}}^{T_{end}} C \, dt, \qquad (1)$$

where the end time, T_{end}, is set to be 30 min.

The bar charts of concentration in g m^{-3} at 9 different SKC locations (summarized in Fig. 14) is shown in Fig. 19, which should be examined in conjunction with Fig. 20, in which the concentration unit is CFU per Liter of Air. Note that in Fig. 19, SKC-1 and LO are at the same location, both of which were at the center of the desk where the sealed envelope was placed. However, the concentrations at SKC-1 and LO in Fig. 20 are slightly different, with the concentration at LO being the largest in the experiment (Trial 3). It is seen from Fig. 19 that the concentration level at SKC-2 (or CW1) is the second largest due to its proximity to LO. The concentration levels at SKC-7 (in the hallway), SKC-8 (in Area II) and SKC-9 (in the exit area) are of the same order of magnitude, all of which are slightly smaller than that at SKC-2. However, concentrations at the above-mentioned 3 locations are reduced drastically in Figs. 28 and 33 for Scenario 1 (to be shown later), for which the front door in Area I is closed after t = 5.5 sec. Consistent with the concentration contours shown in Fig. 17, concentrations at SKC-3 to SKC-6 are significantly smaller than those at the other locations owing to their greater separation from LO. The concentration level at LO is O(10^2) larger than that at SKC-2 in the experiment, which differs markedly from the current simulation which shows that [$C_{LO}/C_{SKC\text{-}2} \approx$ O(10^3)]. Here O(10^n) means 'of the order of magnitude of 10^n', where n is an integer. In contrast, concentration levels at SKC-7 to SKC-9 from the experiment are quite similar, which is in good agreement with our numerical predictions (cf. Fig. 19).

Another major difference shown in Figs. 19 and 20 is that concentration levels at SKC-3 to SKC-6 in the experiment are not insignificant compared to those at SKC-7 to SKC-9. This might be due to (1) the draft from leakage in the windows and walls of the Open Office in Building 13, and (2) BG spores re-entering the study area through the HVAC system not being accounted for in the simulation.

The time histories of concentration at the locations of the high-resolution (HR) slit sampler in g m^{-3} (present calculations) and in ACPLA (experimental measurements) are shown in Figs. 21 and 22, respectively. It can be seen from Fig. 21 that the concentration at the LO is much larger than that at CW1, which attains the second largest concentration shown in the figure. In contrast, from Fig. 22, it can be seen that the concentration at HR-H (or LO in Fig. 21) is only about two times larger than that at HR-G (or CW1 in Fig. 21). As mentioned before, the conversion between g m^{-3} and ACPLA is not known owing to the fact that the number of spores in each colony forming unit (CFU) is not known. Therefore, it is difficult to make an unambiguous comparison between the numerical predictions and the experimental measurements. Nevertheless, to ensure that global mass conservation in the present simulation is satisfied, the total mass released from the source (at the LO position) for $t \geq 10$ sec is calculated by integrating the concentration over the volume of the entire study area, which we found to be equal to 0.102 g. This value is very close to the total mass of 0.1 g released from the source. After checking the global mass conservation in our calculations, we postulated that the above-mentioned discrepancy could be caused by

1. only one control volume with a length scale of about 8.7 cm was used in the present simulation to represent the source (i.e., the letter containing the BG spores);
2. the release period of 10 sec was arbitrarily assumed;
3. deposition and re-suspension of BG spores were not accounted for in the simulation.

Qualitatively speaking, the general trends observed at CW1 (or HR-G), CW2 (or HR-F) and Exit (or HR-E) in Figs. 21 and 22 were similar. The concentration level at CW2 is the smallest among the four HR locations examined. This is because (1) the separation between LO and CW2 is the largest, and (2) the flow velocity in the x- (or LO-to-CW2) direction is rather small ($\approx$ - 0.2 cm s^{-1}) as shown in Fig. 3 earlier. Furthermore, it can be seen from Figs. 21 and 22 that the concentration level at Exit is the second smallest for this scenario because (1) the separation between LO and Exit is smaller than that between LO and CW2, and (2) the front door in Area I is open during the test. Animations of stream traces and contours of concentration for this case are available in the file S0_HVAC_on_35_1800_cs.avi on the attached CD-ROM. It should be noted that in Figs. 29 and 35 for Scenario 1 (to be shown later) the concentration level at Exit is extremely small because the front door in Area I is closed after t = 5.5 sec.

Similar time histories of concentration at the nine locations of the low-resolution (LR) slit samplers (marked in Fig. 14) are exhibited in Figs. 23 and 24 for the numerical predictions and the experimental measurements, respectively. The general trend for the cloud arrival time at each location is comparable in Figs. 23 and 24. For example, the cloud arrival time at LR-2 consistently occurs at the earliest time, again due to the

proximity of this sampling location to the LO. However, some minor differences exist in the predicted and measured results. The cloud in the experiment arrives at LR-8 earlier than it does in the simulation as can be seen from Fig. 23. Unfortunately, no experimental data at LR-9 is available for this scenario. The velocity field near the exit door in the present simulation is almost stagnant (zero) because the boundary there is treated as a "solid wall" (viz., the exit door is perfectly sealed). However, the exit door in the experiment is made of polyethylene sheets to facilitate the experimental personnel exiting and entering the exit door for the other scenarios. It is very possible that air flow leakage at the exit door can be the cause for the above-mentioned discrepancy at LR-8. Both numerical predictions and experiment suggest that cloud arrival times to LR-6 (in the hallway) and LR-7 (in Area II) are very similar, and the concentration level at LR-6 is larger than that at LR-7. Finally, it is noted in the title of Fig. 24 that the letter was opened at 12:42:00 for Trial 3. However, the time history at LR-1 seems to suggest that the letter was opened at 12:36:00. The reason for this inconsistency in the experiment is unknown, but it may be that the timing mechanisms on the various sampling systems used in the experiment were not properly synchronized.

4.2 Scenario 1:

For this scenario, two additional personnel (CW1 and CW2) were involved. A source of 0.1 g of BG spores in a sealed envelope was located at the location of the "Letter Opener" (LO) shown in Fig. 14, which is the same location as in Scenario 0. The experimental personnel (LO, CW1 and CW2) were located initially in front of the tables (marked by Letter Opener, Co-worker 1 and Co-worker 2 in Fig. 14) by about 50 cm. The HVAC system was turned on for about 15 minutes until the flow reaches a pseudo-steady state condition, after which the BG spores were released by opening the sealed envelope. The latter process was assumed to take 10 sec. Immediately after the BG spores were released from the opened envelope, LO, CW1 and CW2 began to walk along the footprint pathway (trail) laid out on the floor of the study area as indicated in Fig. 25, finally exiting through the exit door. The speed of walking of each person was around 1 m s^{-1}. It takes about 12, 11 and 28 sec for LO, CW1 and CW2 to exit through the exit door, respectively. The HVAC system is shut down in the simulation when CW1 passes the HVAC room (at t =5.5 sec). The front door in Area I (close to the Co-worker 1 location in Fig. 14) was closed when the LO passes through it. The rear door in Area I was left open during the simulation in order to satisfy "global mass conservation" in the study area (Areas I to IV plus the hallway). Although the flow rates in cubic feet per minute (CFM) from all supply and return ducts are provided by the experimental measurements and have been adjusted slightly to satisfy

$$\sum \mathrm{CFM}_{\text{supply ducts in study area}} = \sum \mathrm{CFM}_{\text{return ducts in study area}}, \tag{2}$$

mass conservation is not necessarily satisfied in Area I alone from the measurements; i.e.

$$\sum \mathrm{CFM}_{\text{supply ducts in Area I}} \neq \sum \mathrm{CFM}_{\text{return ducts in Area I}}. \tag{3}$$

Eq. (3) represents exactly the condition that persists when both front and rear doors in Area I are closed, causing numerical convergence problems in the simulation. For this reason, the rear door is left open throughout the simulation, which lasts for 30 minutes. This is the same time interval over which the low-resolution (LR) slit samplers were activated in the experiment.

Two cases were considered here for Scenario 1. For Scenario 1a, the HVAC system was turned on throughout the simulation. For Scenario 1b, the HVAC system was shut down by CW1 at time t = 5.5 sec. Note that Scenario 1a is performed as a complementary study (since no experimental data is available for this case) to Scenario 1b in order to see the effect of the HVAC system on the dispersion of the BG spores from the opened envelope. At t = 8.75 sec, the BG concentration contours displayed in Figs. 26 and 31 for these two scenarios are very similar. This is because the HVAC system has just been turned off at t = 5.5 sec in Fig. 31. At t = 30 min, however, Fig. 27 shows that the dispersion of BG spores in the study area is very effective when the HVAC system is turned on all the time, as the cloud is seen to disperse throughout Area I, then spread through the rear door and reach Areas IV, III and II through doors in the hallway. In contrast, as clearly seen in Fig. 32, the dispersion of the BG spores in the Open Office at t =30 min (after the release) is still limited primarily to Area I when the HVAC system was shut down soon after the release of BG spores from the opened letter. This suggests that the advective mechanism, associated with the directed flow motion, is more important than the turbulent diffusive mechanism for the dispersion of BG spores under these indoor conditions. Note that shutting down the HVAC system not only reduces the mean flow motion, but also the level of turbulence in the Open Office. Since the turbulent diffusion coefficient Γ ($\propto \frac{k^2}{\varepsilon}$, where k is the turbulence kinetic energy and ε is the dissipation rate of turbulence kinetic energy) is closely linked to the level of turbulence kinetic energy, shutting down the HVAC system can be a very effective means for reducing the dispersion of BG spores in the office owing to the fact that both advective and diffusive mechanisms for dispersion are being suppressed simultaneously.

If the HVAC system is turned on as in Scenario 1a, it is very important to close both the front and rear doors to prevent the spread of BG spores from Area I to the other areas in the Open Office, including the hallway. It is interesting to compare Figs. 27 and 17 (Scenario 0) in order to see the effect of closing the front door in Area I on the dispersion of BG spores. As expected, when the front door is closed, the concentration contours in Fig. 27 show that the BG spores do not even disperse to the end of the exit area after t = 30 min. Although we were unable to simulate a scenario where both doors in Area I were closed due to the fact that flow rates for both return and supply ducts were only measured when both doors were opened, it is expected that most BG spores from the opened envelope will be “trapped” (and hence confined) inside Area I. Note that BG spores can also enter the return ducts in Area I and, through the HVAC system if it is turned on, re-enter the hallway and Areas II to IV through the supply ducts. However, this mechanism was not considered in the present numerical study.

The bar charts of concentration for Scenarios 1a and 1b are shown in Figs. 28 and 33, respectively, which should be examined in conjunction with Figs. 27 and 32. With the HVAC system turned on all the time (Fig. 28), the concentration levels at SKC-2 to SKC-4 are larger than those with the HVAC system turned off after t = 5.5 sec (cf. Fig. 33). In fact, the concentration levels at SKC-3 to SKC-9 in Fig. 33 are less than 10^{-4} g m^{-3}. Fig. 33 can only be compared qualitatively with Fig. 34 (Trial 3 experiment) because the units of concentration are different (g m^{-3} compared to CFU per Liter of Air). As in Fig. 20, SKC-1 and LO in Fig. 34 correspond to two different samplers that are at slightly different locations on the table shown in Fig. 14. However, SKC-1 and LO in Fig. 33 (simulation) represent exactly the same location, both of which are at the center of the table. One encouraging result here is that $C_{LO}/C_{SKC\text{-}2} \approx O(10^3)$ for both the experimental measurements and the numerical simulation. It can be seen from Fig. 34 that the concentration levels at SKC-2 and SKC-3 are comparable, which contradicts the numerical prediction shown in Fig. 33 (where the concentration level at SKC-3 is much smaller than that at SKC-2). Since the HVAC system is turned off most of time in the experiment and in the Scenario 1b simulation, it is quite unlikely that the concentration level at SKC-2 (which is nearby LO) can be comparable to that at SKC-3. Again, it is surmised that the air flow leakage through the building shell is the primary cause for the above-mentioned difference.

The time histories of concentration at the HR locations for Scenarios 1a and 1b are shown in Figs. 29 and 35, respectively. Note that the range of the y-scale in both figures is different. At t = 10 min (after the release) for example, the concentration level at LO in Fig. 29 (HVAC was turned on all the time) is about 25% of that in Fig. 35 (HVAC is turned off after t = 5.5 sec). This is because advection plays an important role in the dispersion of BG spores; hence, the rapid reduction in the concentration level at LO in Fig. 29. Consistent with this argument is that the cloud arrival time and the level of concentration at CW1 in Fig. 29 occurs earlier and is larger than that in Fig. 35. Note that in both figures, the concentration levels at Exit are insignificant, which is due to the fact that the front door in Area I is closed after t = 5.5 sec. Similar results were observed at HR-H (or Exit) in Fig. 36 in that the level of concentration there was insignificant when compared to the other 3 HR locations. It is also observed in Fig. 36 that the cloud arrives at HR-F (or CW2) about 4 min after the cloud arrives at HR-G (or CW1). Once the concentration levels reach their peak values at both locations, they stay almost at the same level for the remaining time. This explains why the concentration in CFU per Liter of Air at SKC-2 (or HR-G) and SKC-3 (or HR-F) in Fig. 34 are very comparable.

Although it is inappropriate to compare the concentration time histories in Fig. 30 (Scenario 1a, in which the HVAC system is turned on throughout the simulation) and Fig. 39 (corresponding to the experiment, in which the HVAC system was turned off when the experimental personnel leaves Area I), it is interesting to point out that the concentration levels at LR-1 and LR-2 approach each other several minutes after the BG spores were released from LO. In contrast, Fig. 37 (linear scale along the y-axis) and Fig. 38 (logarithmic scale along the y-axis) show that the concentration level at LR-1 is $O(10^2)$ larger than that at LR-2. This observation suggests that the effect of a possible

draft from leakage in the windows and walls of the building shell is probably as strong as the effect arising from the HVAC system.

Since the HVAC system is turned off and the front door in Area I is closed at t = 5.5 sec (after the release) in the simulation for Scenario 1b, it is not surprising to see in Figs. 37 and 38 that the concentration levels for samplers in the hallway, Areas II to IV, and the exit area are very small ($< 10^{-5}$ g m^{-3}). However, Fig. 39 shows that the concentration levels at LR-8 and LR-9 (in the exit region) are about 1 ACPLA, which are 20% of the peak concentration value at LR-1. The possible explanation for this is that a portion of BG spores were deposited on LO and then re-suspended and dispersed into the air as LO walked through the front door in Area I and then exited through the exit door. Furthermore, it can be seen from Fig. 39 that the concentration levels at the other LR locations in Areas II to IV are much smaller than those in the exit region.

Finally, it is instructive to compare the experimental concentration time histories at HR-E (Fig. 36) and LR-1 (Fig. 39) in terms of their peak and "pseudo-steady" state values. Note that samplers corresponding to HR-E and LR-1 are on the same table where the BG-tainted letter was opened. Although the concentration levels at HR-E and LR-1, in Figs. 36 and 39, respectively, reach their corresponding peak values at almost the same time, their peak values in terms of ACPLA are very different: namely, $(C_{\text{HR-E}}/C_{\text{LR-1}})_{\text{peak}} \approx 17$. This ratio drops sharply to $C_{\text{HR-E}}/C_{\text{LR-1}} \approx 2$ at $t \approx 20$ min.

4.3 Scenario 2:

The major difference between Scenarios 1 and 2 is that in Scenario 2, CW1 and CW2 leave Area I, close the front and rear doors, respectively, and exit through the exit door immediately after the BG spores were released from the opened envelope. The LO remains still for 5 min before he too exits the test area following the same footprint pathway on the floor as indicated in Fig. 25. Since we only have flow rate measurements for supply and return ducts when all the doors in Area I were opened in accordance with the SF_6 experiment, numerical convergence problems occur if all doors are closed as mentioned in the discussion following Eq. (3) earlier. In the present simulation, the front door was closed only after the LO leaves the test area. The rear door of Area I was left open throughout the test.

Figs. 40 to 43 show contours of concentration at t = 8.75 sec (BG spores were still being released while the LO remains still after opening the envelope), at t = 185 sec (BG spores were no longer releasing from the opened envelope while the LO remains still), at t = 310.75 sec (the LO is about to exit through the exit area), and at t = 30 min. The concentration contours in Figs. 40 and 16 (Scenario 0) were almost identical. The only difference is that in Fig. 40, CW1 and CW2 have already left Area I. Since CW1 and CW2 leave the test area at a walking speed of about 1 m s^{-1}, which is much faster than the rate at which BG spores are dispersing near the LO, their motions practically cause no disturbance to the dispersion of BG spores. In this simulation, both doors in Area I were open for the first 5 min. As a result, it is seen from Fig. 41 (t < 5 min) and Fig. 42

(t > 5 min) that the BG spores have already dispersed into the hallway near the exit area. At the end of simulation (t = 30 min) as shown in Fig. 43, a portion of the BG spores which were locked out from Area I in Fig. 42, have already spread in both directions from near the front door towards the exit area (to the right) and towards Areas II and III (to the left). Area IV is the only area for which the BG spores have not dispersed into.

Although BG spores have already dispersed into most parts of the study area as shown in Fig. 43 in terms of concentration contours on a logarithmic-scale, the concentration levels at the SKC locations as seen in the bar charts of Fig. 44 show that at most sampler locations (SKC-3 to SKC-9) the concentration was below 10^{-4} g m^{-3}, with the exception of the locations at SKC-1 (or LO) and SKC-2 (or CW1). It is informative to compare Fig. 33 (where the front door was closed after t = 5.5 sec) and Fig. 44 (where the front door was closed after t = 5 min 5.5 sec). For both cases, the HVAC system was turned off after t = 5.5 sec. The concentration levels at LO and SKC-2 in both figures are very comparable, although concentration at SKC-2 in Fig. 33 is slightly smaller than that in Fig. 44. This might be due to the presence of the LO for the first 5 min being able to obstruct (or, restrict) the spread of BG spores in the case of Fig. 44 (see also Figs. 31 and 40 for the corresponding concentration contours at t = 8.75 sec).

The experimental data (Trial 3) for this scenario, shown in Fig. 45 in CFU per Liter of Air instead of in g m^{-3}, is quite different from the numerical predictions, especially in terms of $C_{LO}/C_{SKC\text{-}2}$. The predicted $C_{LO}/C_{SKC\text{-}2}$ is O(10^3) and $C_{LO}/C_{SKC\text{-}2}$ from the experimental measurements is O(10). It should be noted here that $C_{LO}/C_{SKC\text{-}2} \approx$ O(10^3) in Scenario 1 for both the numerical predictions and the experimental measurements. The major difference between Figs. 34 and 45 is that the concentration levels at SKC-2 and SKC-3 in the present scenario as shown in Fig. 45 are O(10) larger than those shown in Fig. 34 (Scenario 1). Also, the concentration level at LO shown in Fig. 45 is O(10) smaller than that shown in Fig. 34. Since the HVAC system was turned off in both experiments, it is possible that the discrepancy can be attributed to the air flow leakage from windows and walls in the building shell, particularly in Scenario 2. Another contributing factor to the discrepancy might be experimental anomaly as shown in Fig. 46, in which $C_{LO}/C_{SKC\text{-}2} \approx$ O(10^2) for Trial 5 and $C_{LO}/C_{SKC\text{-}2} \approx$ O(10) for Trial 3 (an "identical" replication) as seen in Fig. 45.

In this experiment, CW1 and CW2 exit the test area immediately after the LO informs them that he has opened the letter containing the BG spores. Both front and rear doors are closed as soon as CW1 and CW2 leave Area I. However, it is still possible that a small portion of BG spores deposit on CW1 and disperse into the test area outside Area I as CW1 walks along the footprint path shown in Fig. 25. This hypothesis is supported by the reasonably high concentration levels measured at the locations of SKC-4 to SKC-9, which are outside Area I. In contrast, the predicted concentration levels shown in Fig. 44 are less than 10^{-4} g m^{-3} at SKC-4 to SKC-9, because deposition and re-suspension are not considered in the numerical simulation.

The predicted time histories of concentration at the HR locations are depicted in Figs. 47 and 48 on linear and logarithmic scales along the y-axis, respectively. It is observed by

comparing Figs. 35 and 47 that the concentration level at LO in Fig. 35 is generally larger than that in Fig. 47. This is because in Fig. 35 (Scenario 1) the front door is closed after t = 5.5 sec, which prevents the spread of the BG spores from the opened letter outside Area I. In contrast, for the results shown in Fig. 47, the front door was left open for 5 min 35 sec until the LO exits the test area. Note that there is a sharp increase in concentration at $t \approx 5$ min (when the front door is closed). The concentration reaches its peak value at $t \approx 6$ min and then decreases to the minimum value at $t \approx 7$ min before it rises again to reach its second peak at $t \approx 12$ min. In order to provide a possible explanation for the peak concentration value at $t \approx 6$ min, three supplementary figures (Figs. 49 to 51) are provided here to show concentration contours (some superimposed with velocity vectors) on a vertical y-z plane at the LO position at t = 4 min 50 sec (Fig. 49; before the front door is closed), at t = 6 min 22 sec (Fig. 50; after the front door is closed) and at t = 20 min 22 sec (Fig. 51). In Fig. 49, the cloud adjacent to the ceiling is moving towards the front door. In Fig. 50, however, the same cloud is deflected in the reverse direction (i.e., back towards the LO) at t = 6 min 22 sec because the front door is closed. This reverse deflection is probably the reason why the concentration reaches its peak value at $t \approx 6$ min. Examination of Figs. 50 and 51 also shows that the magnitude of the velocity in Fig. 51 (at t = 20 min 22 sec) is much smaller than that in Fig. 50 (at t = 6 min 22 sec). The rapid decay of the velocity magnitude is clearly due to the HVAC system being shut down at t = 5.5 sec. Since there is hardly any flow motion (or advection effect) in Fig. 51, the turbulent diffusion process becomes the dominant mechanism for dispersing BG spores, resulting in a slow decay of the concentration at the LO location for $t > 12$ min as shown in Fig. 47.

The concentration time histories at CW1 and CW2 in Figs. 47 and 48 are better understood in conjunction with Fig. 52 at the corresponding locations (HR-G ≡ CW1 and HR-F ≡ CW2). Consistent with the bar charts of concentration at SKC-2 and SKC-3 in Fig. 45, for which the concentration at SKC-3 from the experiment is slightly smaller than that at SKC-2, the concentration levels at HR-G and HR-F in Fig. 52 become very comparable approximately 8 min after the BG spores were released from the opened letter. This is markedly different from the present numerical prediction, in which the concentration level at CW2 is $O(10^4)$ smaller than that at CW1 at t = 30 min (Fig. 48). As mentioned before, this might be due to the air flow leakage problem in Area I. At Exit (or HR-E), however, both simulation and experiment show that the concentration level there was insignificant in comparison with the concentration level at CW1 (or HR-G).

Finally, the time histories at the LR locations are shown in Figs. 53 and 54 (on linear and logarithmic scales along the y-axis) in g m^{-3} for the present prediction. Fig. 55 displays the associated concentration time histories measured in the experiment in ACPLA. Let us first examine the experimental concentration time history at the LR locations for Scenario 1 (Fig. 39) and the present scenario (Fig. 55). In Fig. 55, a sharp increase of concentration occurs immediately after the letter containing the BG spores was opened (at 13:04:00) at both LR-1 and LR-2. However, in Fig. 39 a sharp increase of concentration at LR-1 is observed at 12:28:00 (i.e., 3 min before the letter was opened at 12:32:00), which is peculiar. At LR-2 in Fig. 39, the concentration starts to increase rapidly approximately at the same time as when the letter was opened, which is consistent with what is seen in Fig.

55 at the same location. Another interesting observation in Fig. 55 is that the concentration at LR-1 is smaller than that at LR-2 within the first 12 min. This seems to suggest that there exists a strong skewed cross flow in the study area from where the letter was opened towards LR-2. It is apparent from the present simulation that such a cross flow does not exist because the cloud arrival time at LR-2 is at $t \approx 6$ min. Also, $C_{\text{LR-1}}/C_{\text{LR-2}} \approx 2.3$ in Fig. 53 instead of $C_{\text{LR-1}}/C_{\text{LR-2}} \approx 1$ as in Fig. 55 at $t = 30$ min. Finally, the concentration levels at LR-3 to LR-9 are much smaller than those at LR-1 and LR-2 for both the numerical simulation and experimental measurements, which is consistent with what we observed earlier in Scenario 1.

5. CONCLUSIONS AND RECOMMENDATIONS

In the present study, two experiments, namely SF_6 and BG release experiments were simulated using CFD. In the SF_6 release experiment, ventilation measurements in terms of volumetric flow rate were conducted, and the time histories of concentration in ppm at 7 sampler locations were available, which, in theory, are reproducible by CFD if the laboratory environment (study area) is well controlled (viz., if there is no air flow leakage in the test area). The BG release experiments, however, were much more challenging to simulate because the concentration unit adopted in the experimental measurements (e.g. CPU per Liter of Air or ACPLA) cannot be related unambiguously to the mass of BG spores released in the opened letter. More specifically, the number of spores in the sealed envelope in colony forming unit (CFU) was unknown, and the actual number of BG spores released when the letter was opened is also unknown. Therefore, we can only make qualitative rather than quantitative comparisons between the numerical predictions and the experimental measurements of BG concentration because the exact conversion between CPU per Liter of Air, ACPLA and g m^{-3} were unknown. In the case of the BG release experiments, three different scenarios were simulated here, and two of them involved experimental personnel leaving the test area. In order to numerically model one or more people leaving the office, a first-order Immersed Boundary Method (IBM) was implemented in the CFD flow solver STREAM. Overall, CFD is able to generate very realistic flow and concentration fields in the indoor environment, even with the HVAC system turned off at an early stage in the experiment and experimental personnel moving in the test area. The test calculations permitted the following conclusions to be drawn and recommendations to be made.

For the SF_6 experiment, we believed that the flow rate measurements for supply and return ducts are accurate. Therefore, it is hypothesized that the discrepancy between the numerical predictions and experimental measurements of concentration were mainly caused by

1. air flow leakage from cracks and crevices in the walls and windows of the building shell;
2. decoupling between the present CFD simulation and dispersion of SF_6 in the HVAC system.

The remedy for point (1) is either to introduce a 'blower door' experiment to determine the locations of the leaks and the air flow rates through these leaks, or to conduct a series of new experiments in an office environment that is certified to be airtight. The remedy for point (2) is to couple the present 3-D CFD model, for simulation of flow and dispersion in an Open Office, with a 1-D zonal model (such as COMIS or CONTAM), to simulate the flow and dispersion in the HVAC system. This CFD/zonal-model coupling should improve the numerical predictions for the SF_6 experiment and Scenario 0 (Baseline Case) in the BG release experiment, in which the HVAC system was turned on throughout the experiment.

For the BG release experiment, it is not possible to make quantitative comparisons between the numerical predictions and experiment measurements of concentration because

1. the exact conversion between ACPLA and CFU per Liter of Air used in the experimental measurements and g m^{-3} used in the simulation was not known;
2. the exact release period and quantity of BG spores released when the envelope was opened was not known;
3. the effect of deposition and re-suspension of BG spores in the indoor environment was not considered in the present CFD simulations.

Moreover, the flow rate measurements for the supply and return ducts were assumed to be the same as those in the SF_6 experiment, which is particularly questionable for Scenarios 1 and 2, in which experimental personnel are moving in the study area and the doors in Area I are closed. In both scenarios, unsteady CFD simulations were performed. Since both front and rear doors in Area I were closed as the experimental personnel exited the test area, the ventilation measurements in Area I alone will need to be changed as suggested in Eq. (3) based on the argument of global mass conservation in Area I. In theory, *time-dependent* flow rate measurements for the supply and return ducts should be made available and used as boundary conditions to perform the CFD simulations. As a minimum requirement to simulate the BG experiment, volumetric flow rates for the supply and return ducts should be measured for the following cases: (a) only the two middle doors in Area I are closed, and (b) all four doors in Area I are closed.

To address point (3) above, it is recommended that the present unsteady RANS approach be combined with an eddy interaction model (EIM, or random walk model) for modeling aerosol dispersion and deposition. EIM is based on a Lagrangian stochastic approach where individual particles are allowed to interact successively with discrete eddies. Each eddy has length, velocity and lifetime characteristic scales obtained from the ensemble-averaged flow and turbulence fields. The end of the interaction between the particle and an eddy occurs when the lifetime of the eddy is over or when the particle crosses the eddy. At this instant, an interaction of the particle with a new eddy begins. The trajectory of this particular particle is obtained by solving the particle equations of motion (see, e.g., [13]). In a simple EIM, the local fluctuating velocities are obtained by multiplying the root-mean-square fluid fluctuating velocity ($u'_{f,rms} = v'_{f,rms} = w'_{f,rms} = \sqrt{2k/3}$) by random numbers generated from a Gaussian probability density function with zero mean and unit

standard deviation at the start of one eddy-particle interaction. Details of EIM can be found in [14,15].

Finally, it should be emphasized here that the advantages of utilization of CFD modeling for assessment and design of mitigation strategies and protocols for defence against anthrax-tainted letters over an experimentally-based approach to the problem are obvious: (1) substantial reduction of lead times and costs of new designs involving other office configurations; (2) ability to study scenarios where controlled experiments are difficult or impossible to perform; and, (3) practically unlimited level of detail of results such as the flow field in the indoor environment and the concentration field of the dispersing BG spores (or, other contaminants) that are released into this flow field.

REFERENCES

1. F.S. Lien and M.A. Leschziner, A General Non-Orthogonal Collocated FV Algorithm for Turbulent Flow at all Speeds Incorporating Second-Moment Closure, Part 1: Computational Implementation, *Comp. Meth. Appl. Mech. Eng.* **114** (1994) 123-148.
2. F.S. Lien and M.A. Leschziner, Upstream Monotonic Interpolation for Scalar Transport with Application in Complex Turbulent Flows, *Int. J. Num. Meth. Fluids* **19** (1994) 527-548.
3. B.P. Leonard, A Stable and Accurate Convection Modelling Procedure Based on Quadratic Upstream Interpolation, *Comput. Meth. Appl. Mech. Eng.* **19** (1979) 59-98.
4. S.V. Patankar, Numerical Heat Transfer and Fluid Flow, McGraw-Hill (1980).
5. C.M. Rhie and W.L. Chow, A Numerical Study of the Turbulent Flow Past an Isolated Airfoil with Trailing Edge Separation, *AIAA J.* **21** (1983) 1525-1532.
6. M. J. Aftosmis, M. J. Berger and J. E. Melton, Robust and efficient Cartesian mesh generation for component based geometry, Tech. Report AIAA-97-0196, U.S. Air Force Wright Laboratory (1997).
7. C. Peskin, Numerical Analysis of Blood Flow in the Heart, *J. Comput. Phys.* **25** (1977) 220-235.
8. Y.H. Tseng and J.H. Ferziger, A Ghost-Cell Immersed Boundary Method for Flow in Complex Geometry, *J. Comput. Phys.* **192** (2003) 593-623.
9. R.E. McCleery (2006), National Institute for Occupational Safety and Health (NIOSH), private communication.
10. COMIS. http://epb.lbl.gov/comis/.
11. CONTAM. http://www.bfrl.nist.gov/IAQanalysis/index.htm.
12. K.J. Hsieh, F.S. Lien and E. Yee (2006), "Numerical Modelling of Scalar Dispersion in an Urban Canopy", *Journal of Wind Engineering & Industrial Aerodynamics* (in revision).
13. I. Kim, S. Elgobashi and W.A. Sirignano, On the Equation for Spherical-Particle Motion: Effect of Reynolds and Acceleration Numbers, *J. Fluid Mech.* **367** (1998) 221-253.
14. D.I. Graham and P.W. James, Turbulent Dispersion of Particles Using Eddy Interaction Models, *Int. J. Multiphase Flow*. **22** (1996) 157-175.

15. L.P. Wang and D.E. Stock, Stochastic Trajectory Models for Turbulent Diffusion: Monte Carlo Process Versus Markov Chains, *Atmospheric Environment* **26** (1992) 1599-1607.

APPENDIX: README for CDROM

Scenario 0 (Baseline)

In "S0_HVAC_on" directory for Baseline Scenario, the HVAC system is turned on during the simulation. The release time for the contaminant (0.1 gram of BG spores) is 10 sec. The unit for concentration C is g m^{-3}. The simulation lasts for 30 minutes. The animation is produced every 1.25 sec for $0 \le t \le 35$ sec. During the time interval $35 \le t \le 1800$ sec, the animation is produced every 1 minute.

File Name	Starting Time	End Time	Display Mode
S0_HVAC_on_0_35_c.avi	$t = 0$ s	$t = 35$ s	Concentration
S0_HVAC_on_0_35_cs.avi	$t = 0$ s	$t = 35$ s	Concentration and stream trace
S0_HVAC_on_0_35_s.avi	$t = 0$ s	$t = 35$ s	Stream trace
S0_HVAC_on_35_1800_c.avi	$t = 35$ s	$t =1800$ s	Concentration
S0_HVAC_on_35_1800_cs.avi	$t = 35$ s	$t =1800$ s	Concentration and stream trace
S0_HVAC_on_35_1800_s.avi	$t = 35$ s	$t =1800$ s	Stream trace

Scenario 1

In "S1_HVAC_off" directory for Scenario 1, the HVAC system is turned off after t = 5.5 sec. The door closest to co-worker 1 is also closed after t = 5.5 sec. The release period for the contaminant (0.1 gram of BG spores) is 10 sec. The unit for concentration C is g m^{-3}. The simulation lasts for 30 minutes. The animation is produced every 1.25 sec for $0 \le t \le 35$ sec, in which all personnel (letter-opener, co-worker 1 and co-worker 2) exits through the exit door. During the interval $35 \le t \le 1800$ sec, the animation is produced every 1 minute.

File Name	Starting Time	End Time	Display Mode
S1_HVAC_off_0_35_c.avi	t= 0 s	t = 35 s	Concentration
S1_HVAC_off_0_35_cs.avi	t = 0 s	t = 35 s	Concentration and stream trace
S1_HVAC_off_0_35_s.avi	t = 0 s	t = 35 s	Stream trace
S1_HVAC_off_35_1800_c.avi	t = 35 s	t=1800 s	Concentration
S1_HVAC_off_35_1800_cs.avi	t = 35 s	t=1800 s	Concentration and stream trace
S1_HVAC_off_35_1800_s.avi	t = 35 s	t=1800 s	Stream trace

In "S1_HVAC_on" directory for Scenario 1 as a complementary study, the HVAC system is turned on during the simulation. The door closest to co-worker 1 is also closed after t = 5.5 sec. The release period for the contaminant (0.1 gram of BG spores) is 10 sec. The unit for concentration C is g m^{-3}. The simulation lasts for 30 minutes. The animation is produced every 1.25 sec for $0 \le t \le 35$ sec, in which all personnel (letter-opener, co-worker 1 and co-worker 2) exits through the exit door. During the interval $35 \le t \le 1800$ sec, the animation is produced every 1 minute.

File Name	Starting Time	End Time	Display Mode
S1_HVAC_on_0_35_c.avi	t = 0 s	t = 35 s	Concentration
S1_HVAC_on_0_35_cs.avi	t = 0 s	t = 35 s	Concentration and stream trace
S1_HVAC_on_0_35_s.avi	t = 0 s	t = 35 s	Stream trace
S1_HVAC_on_35_1800_c.avi	t = 35 s	t=1800 s	Concentration
S1_HVAC_on_35_1800_cs.avi	t = 35 s	t=1800 s	Concentration and stream trace
S1_HVAC_on_35_1800_s.avi	t = 35 s	t=1800 s	Stream trace

Scenario 2

In "S2_HVAC_off" directory for Scenario 2, the HVAC system is turned off after t = 5.5 sec. The release period for the contaminant (0.1 gram of BG spores) is 10 sec. The unit for concentration C is g m^{-3}. The simulation lasts for 30 minutes. The animation is produced every 1.25 sec for $0 \le t \le 35$ sec, in which co-worker 1 and co-worker 2 exits through the exit door. During $35 \le t \le 302$ sec, in which the letter-opener remains still, the animation is produced every 15 sec. The letter-opener exits the test area and the door closest to co-worker 1 is closed for $302 \le t \le 322$ sec, in which the animation is produced every 1.25 sec. From t = 322 to t = 1800 sec, the animation is produced every 1 minute.

File Name	Starting Time	End Time	Display Mode
S2_HVAC_off_0_35_c.avi	t=0 s	t=35 s	Concentration
S2_HVAC_off_0_35_cs.avi	t=0 s	t=35 s	Concentration and stream trace
S2_HVAC_off_0_35_s.avi	t=0 s	t=35 s	Stream trace
S2_HVAC_off_35_302_c.avi	t=35 s	t=302 s	Concentration
S2_HVAC_off_35_302_cs.avi	t=35 s	t=302 s	Concentration and stream trace
S2_HVAC_off_35_302_s.avi	t=35 s	t=302 s	Stream trace
S2_HVAC_off_302_322_c.avi	t=302 s	t=322 s	Concentration
S2_HVAC_off_302_322_cs.avi	t=302 s	t=322 s	Concentration and stream trace
S2_HVAC_off_302_322_s.avi	t=302 s	t=322 s	Stream trace
S2_HVAC_off_322_1800_c.avi	t=322 s	t=1800 s	Concentration
S2_HVAC_off_322_1800_cs.avi	t=322 s	t=1800 s	Concentration and stream trace
S2_HVAC_off_322_1800_s.avi	t=322 s	t=1800 s	Stream trace

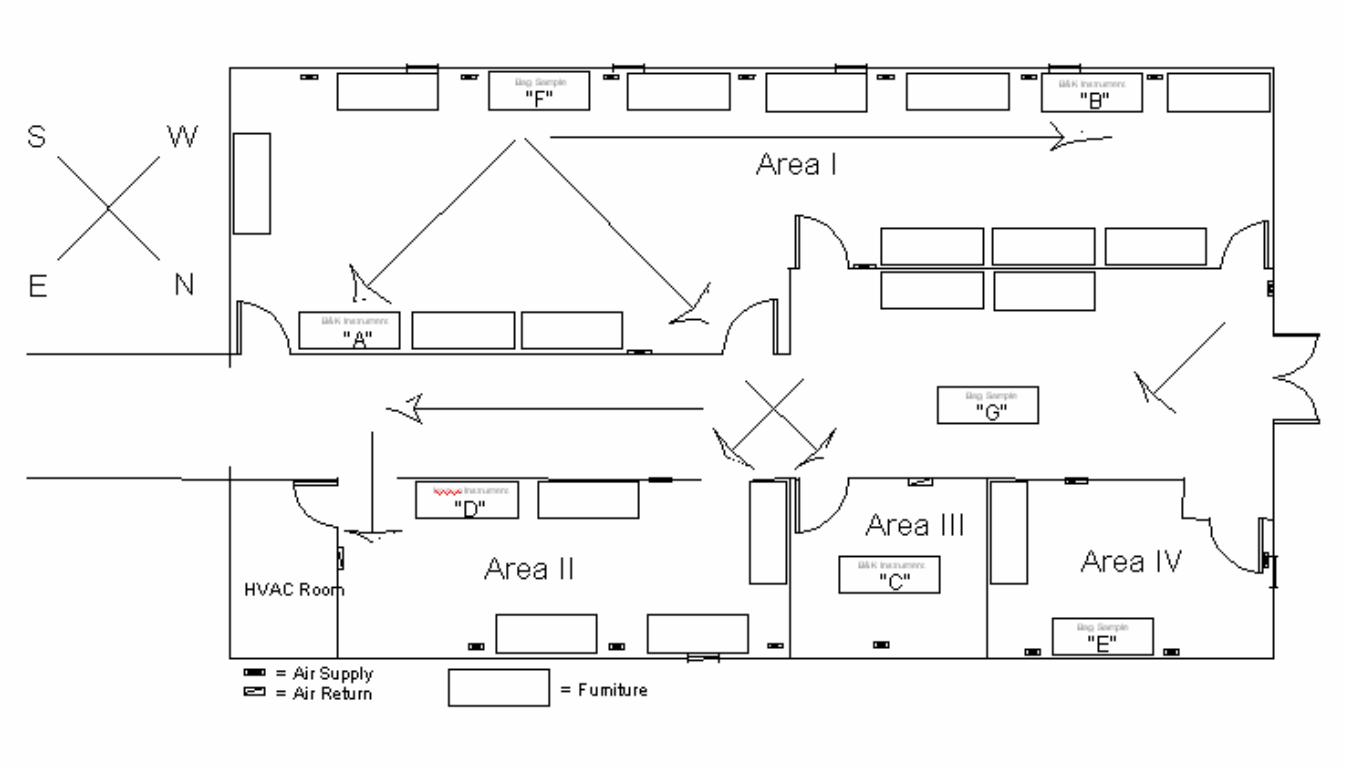

Figure 1: Study area in Building 13 with sampling locations, furniture layout and air flow from the SF_6 experiment.

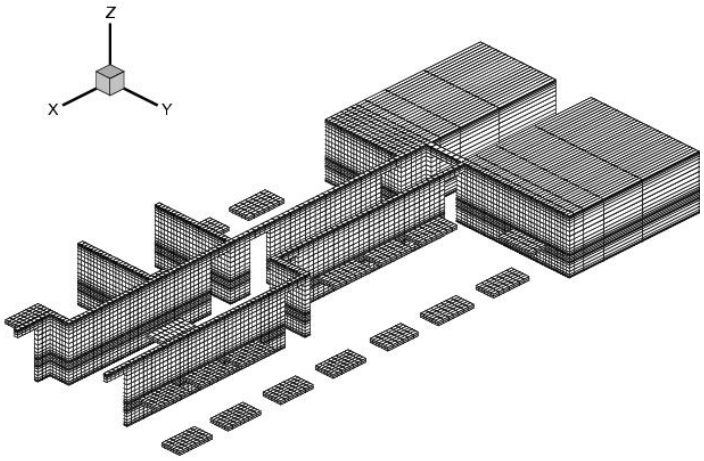

Figure 2: Grid and geometry used by CFD to simulate the SF_6 experiment.

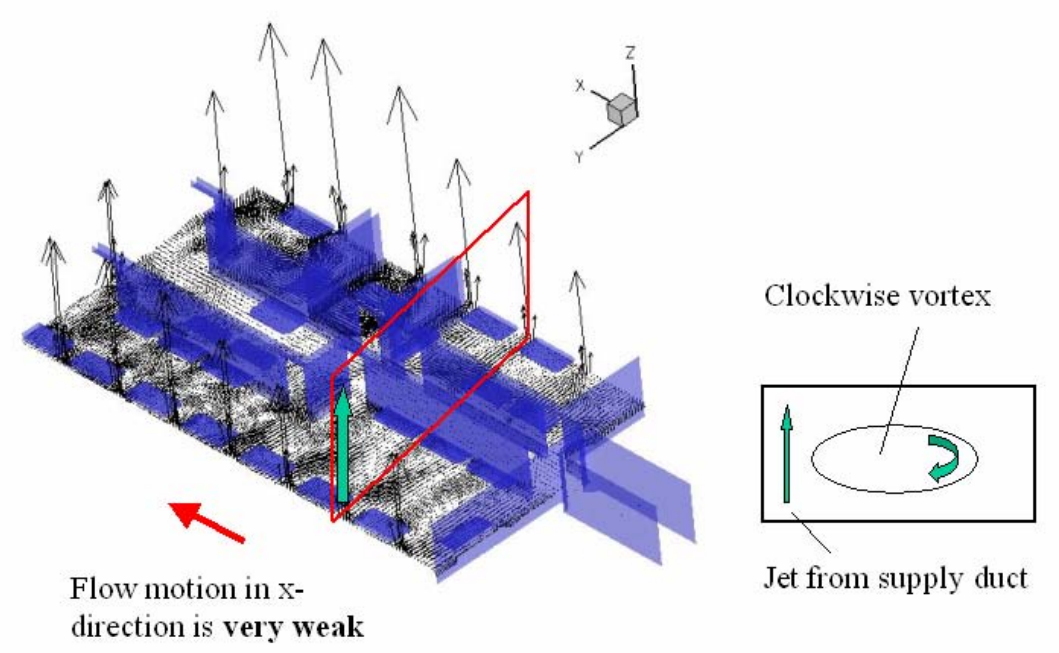

Figure 3: Predicted vortex pattern on a vertical *y-z* plane for the SF_6 experiment.

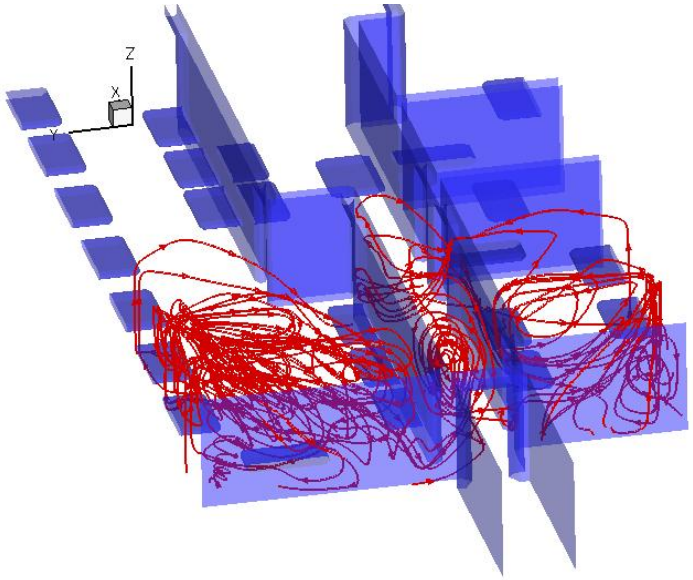

Figure 4: Predicted stream traces in Area I near LO for the SF_6 experiment.

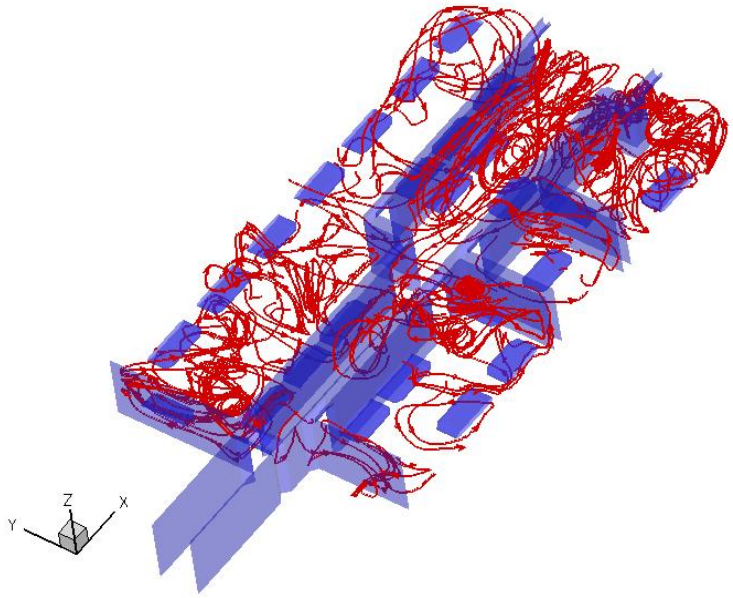

Figure 5: Predicted stream traces in the study area in Building 13 for the SF_6 experiment.

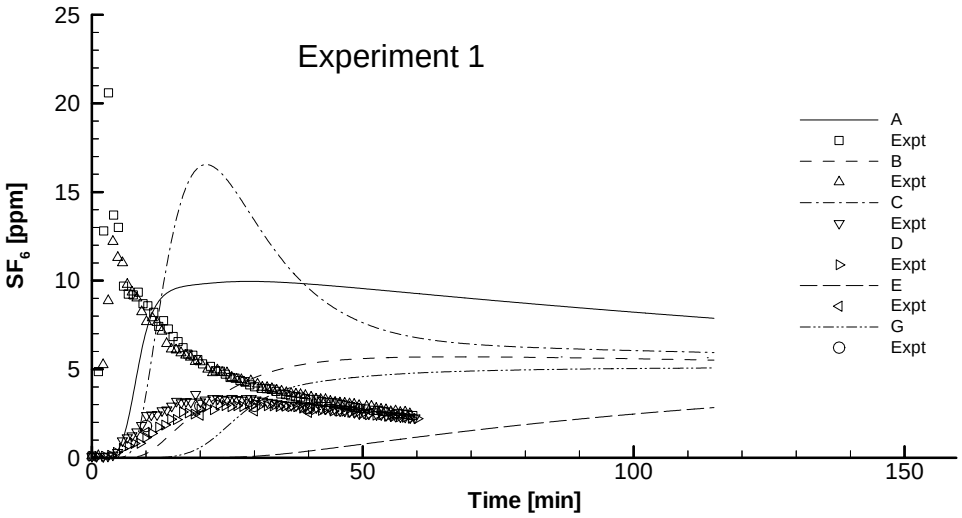

Figure 6: Time histories of concentration in ppm from the CFD predictions compared with experimental measurements for the SF_6 experiment.

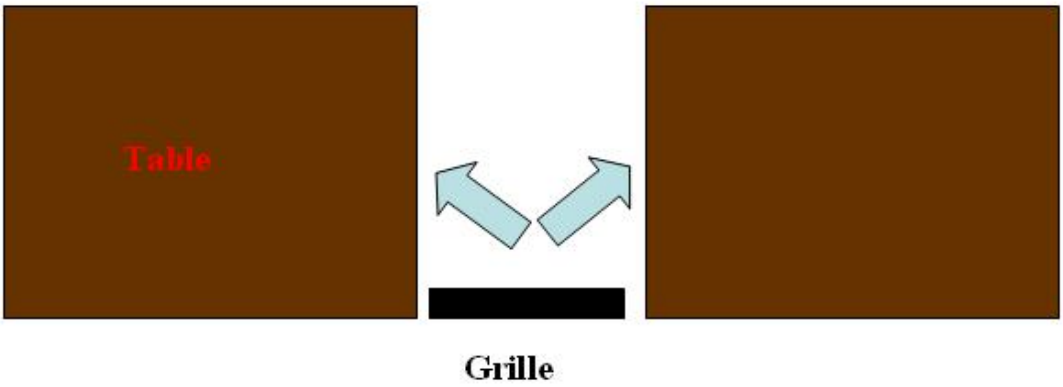

Figure 7: Deflection of airflow by grille on a supplied duct.

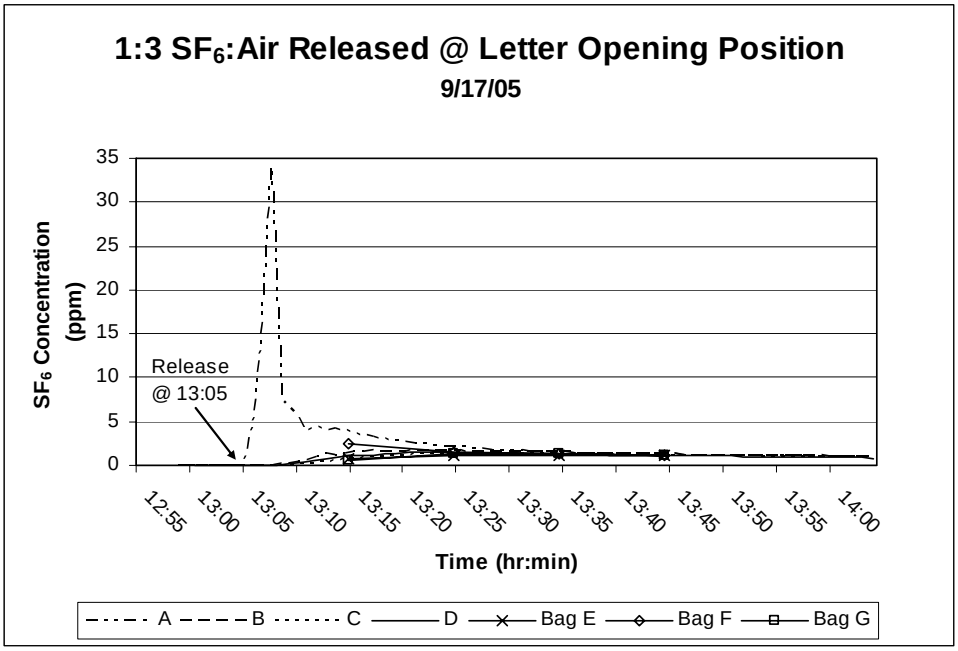

Figure 8: Tracer Gas Experiment 5: 4.0 Liters of 1:3 (pure SF_6:air) released into room by a sampling pump [1].

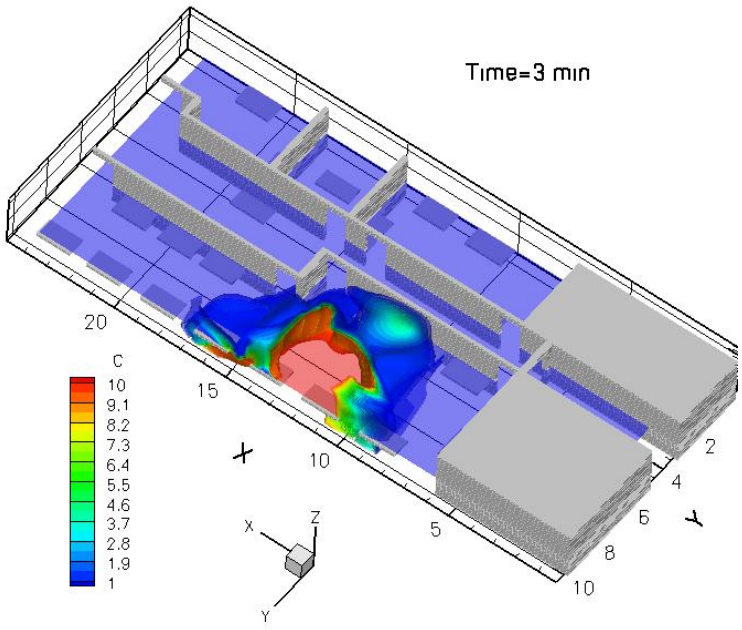

Figure 9: Iso-surfaces of concentration in ppm from the CFD predictions at *t* = 3 min for the SF_6 experiment.

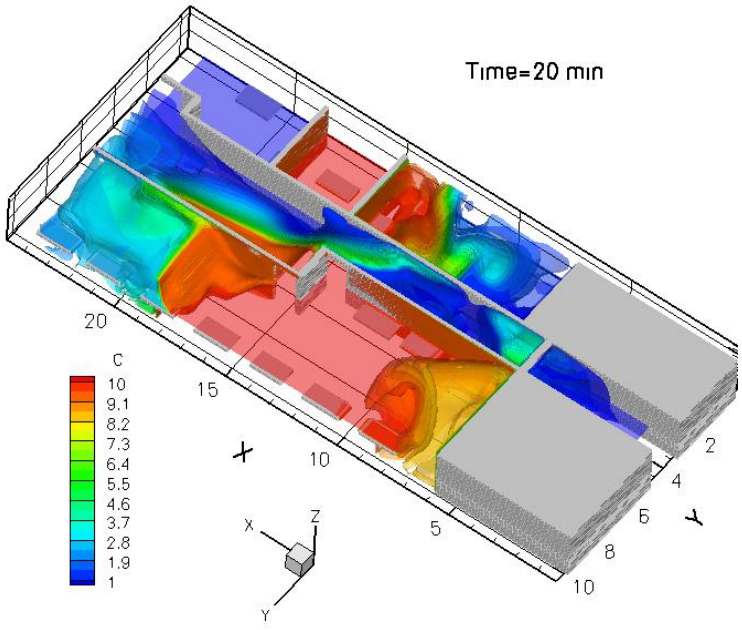

Figure 10: Iso-surfaces of concentration in ppm from the CFD predictions at *t* = 20 min for the SF_6 experiment.

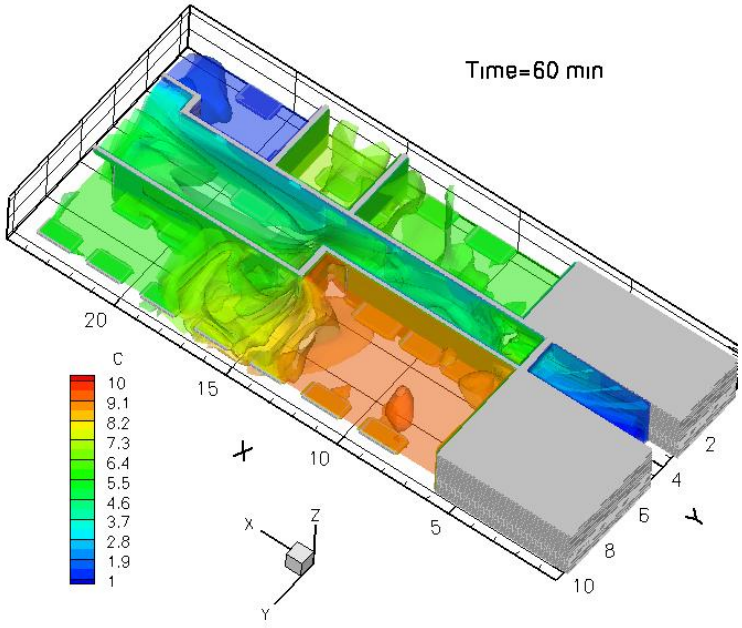

Figure 11: Iso-surfaces of concentration in ppm from the CFD predictions at *t* = 60 min for the SF_6 experiment.

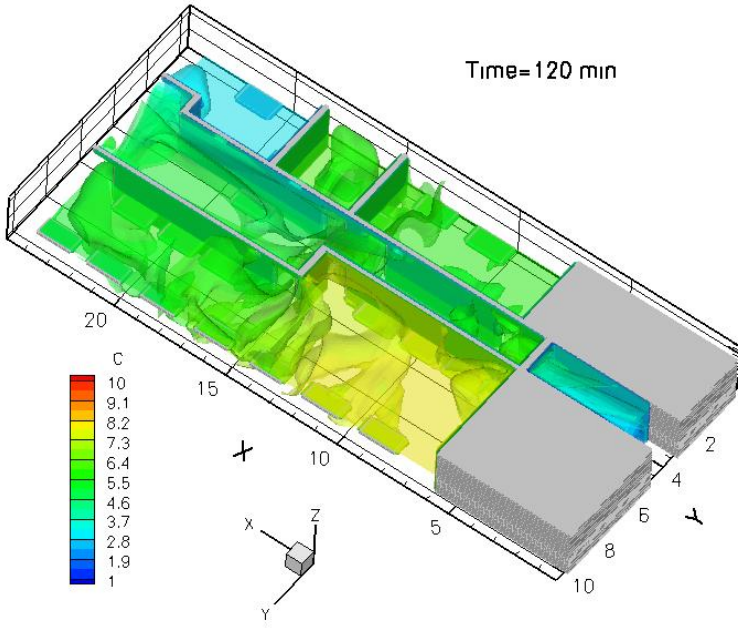

Figure 12: Iso-surfaces of concentration in ppm from the CFD predictions at *t* = 120 min for the SF_6 experiment.

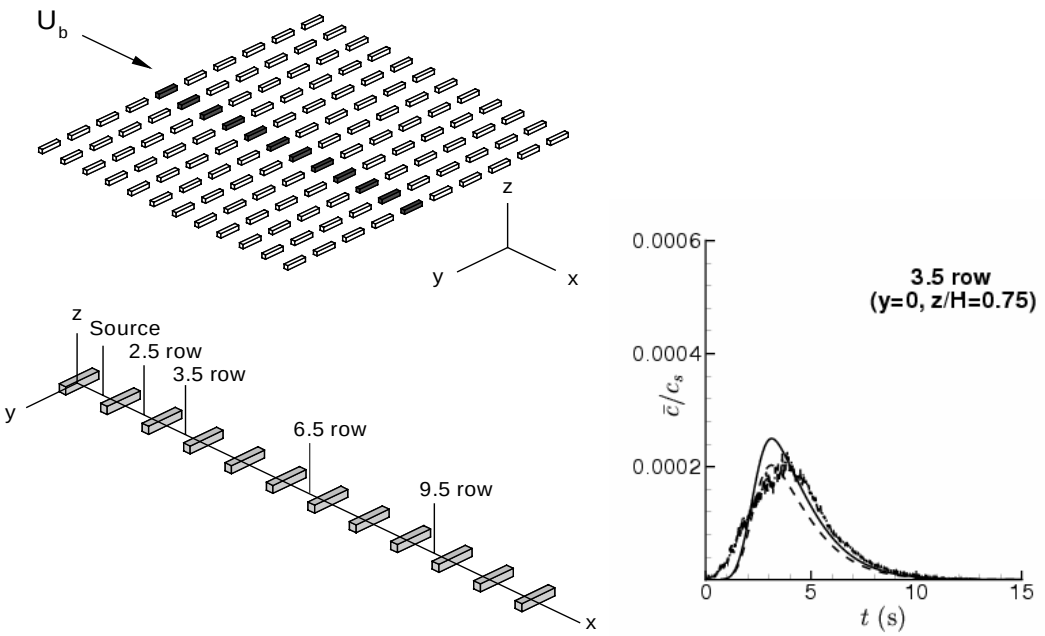

Figure 13: Time history of the normalized mean concentration profile along the vertical center plane of an obstacle array (y = 0) and at z/H = 0.75. Solid and dashed lines: predictions; dash-dot line: experiment [4].

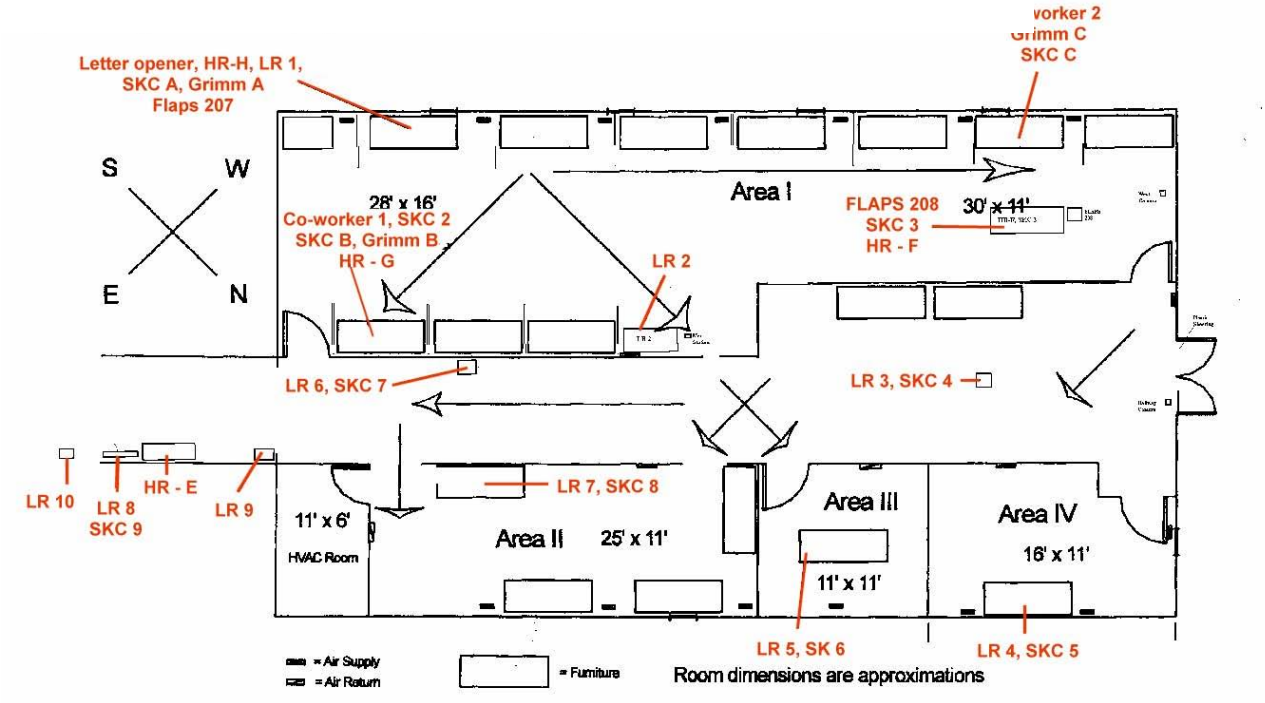

Figure 14: Study area in Building 13 with sampling locations, furniture layout and air flow from the BG experiment.

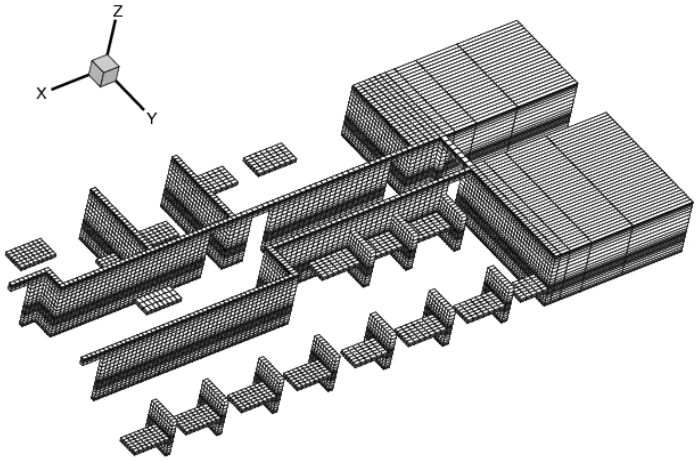

Figure 15: Grid and geometry used by CFD to simulate the BG experiment.

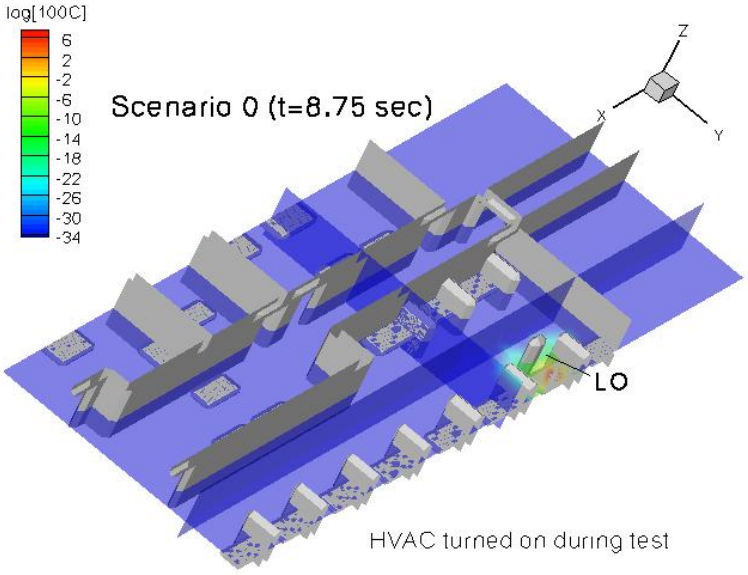

Figure 16: Contours of concentration for Scenario 0 (Baseline Case) at *t* = 8.75 sec.

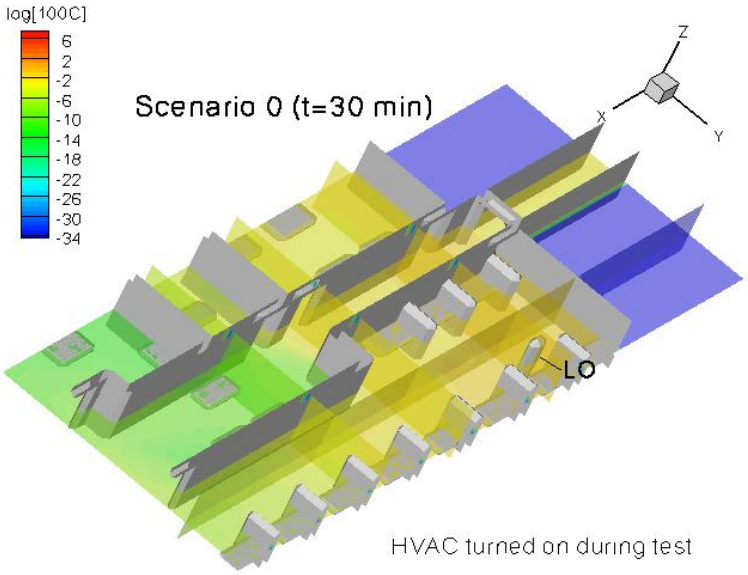

Figure 17: Contours of concentration for Scenario 0 (Baseline Case) at *t* = 30 min.

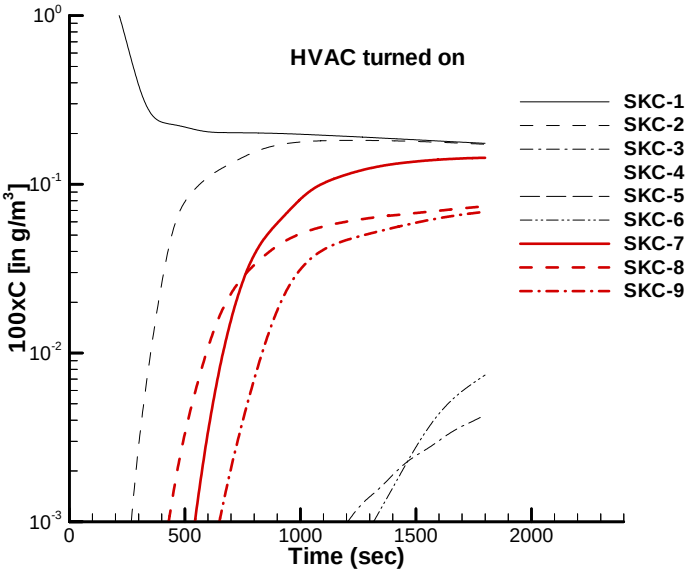

Figure 18: Time histories of concentration at the SKC locations for Scenario 0 (Baseline Case).

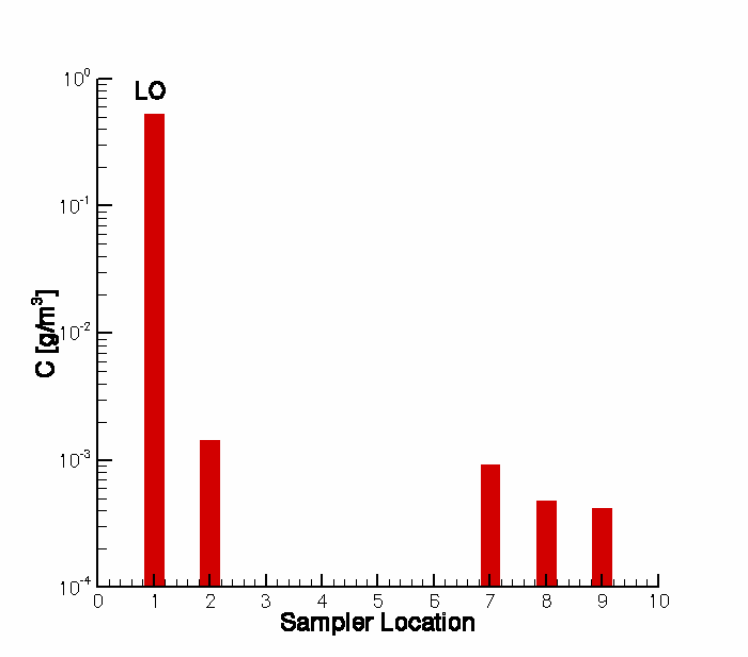

Figure 19: Bar charts of concentration in g m^{-3} at the SKC locations for Scenario 0 (Baseline Case).

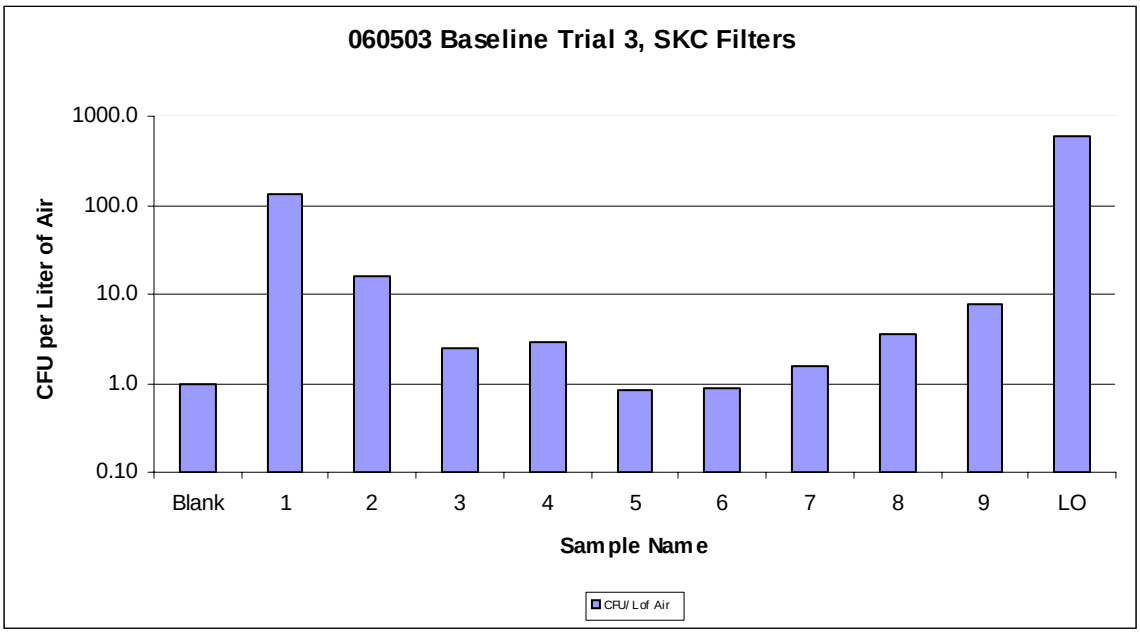

Figure 20: Bar charts of concentration from experiment (Trial 3) in CPU per Liter of Air at the SKC locations for Scenario 0 (Baseline Case).

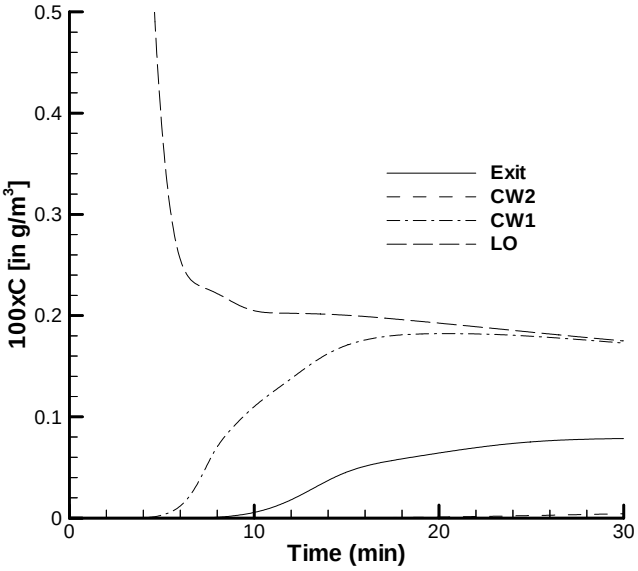

Figure 21: Time histories of concentration in g m^{-3} at the HR locations for Scenario 0 (Baseline Case).

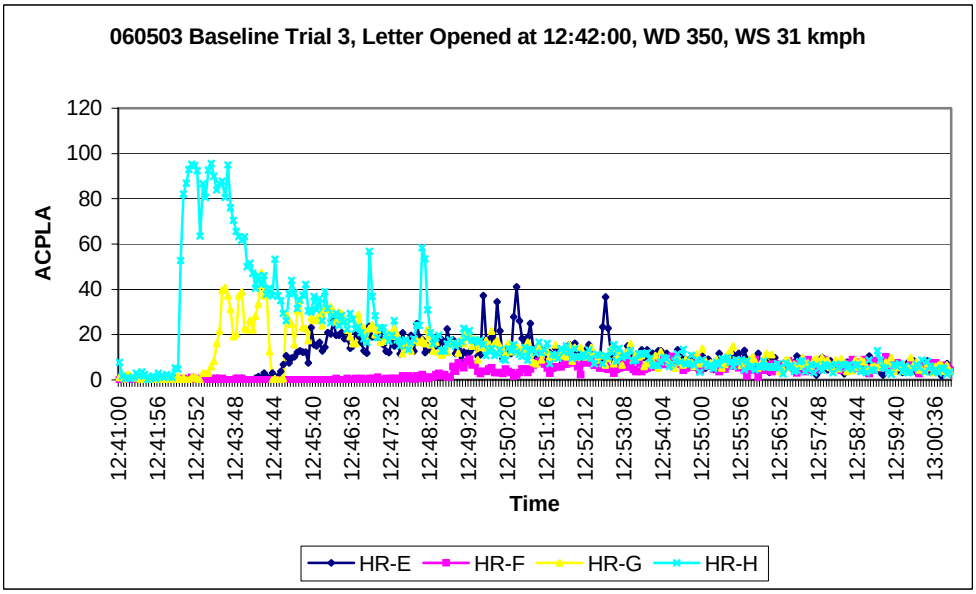

Figure 22: Time histories of concentration in ACPLA from experiment (Trial 3) at the HR locations for Scenario 0 (Baseline Case).

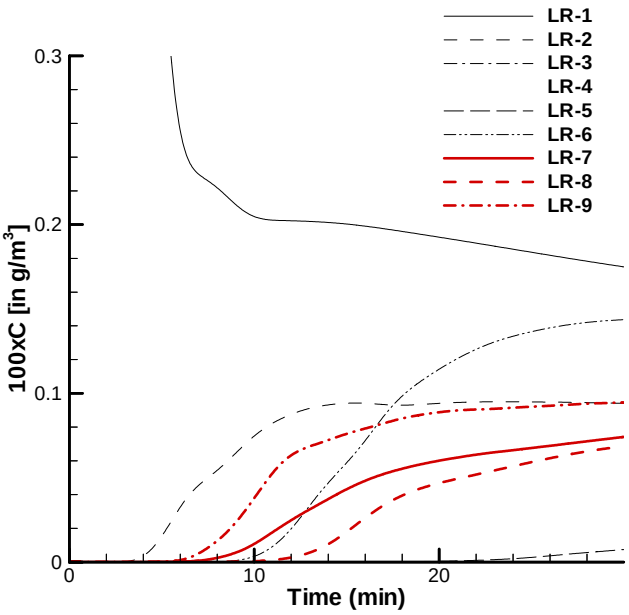

Figure 23: Time histories of concentration in g m^{-3} at the LR locations for Scenario 0 (Baseline Case).

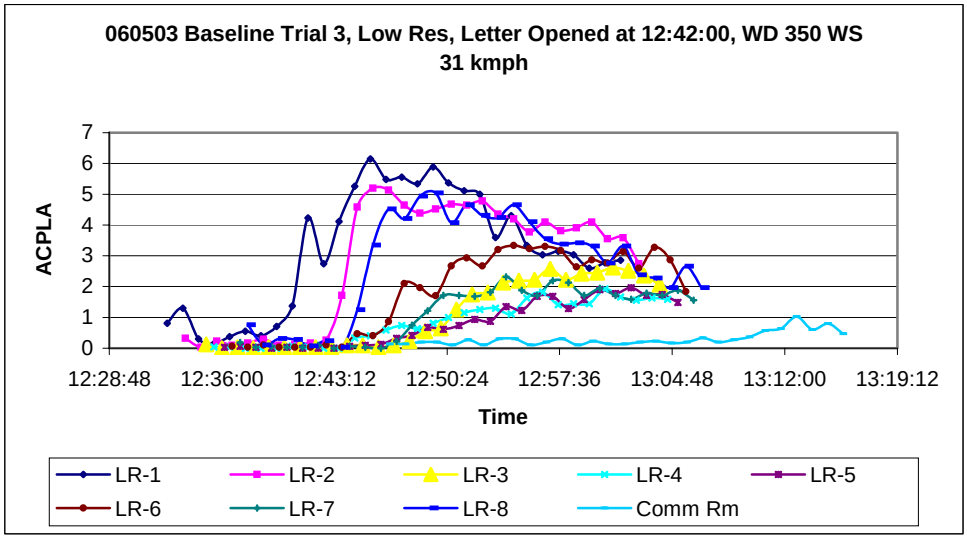

Figure 24: Time histories of concentration in ACPLA from experiment (Trial 3) at the LR locations for Scenario 0 (Baseline Case).

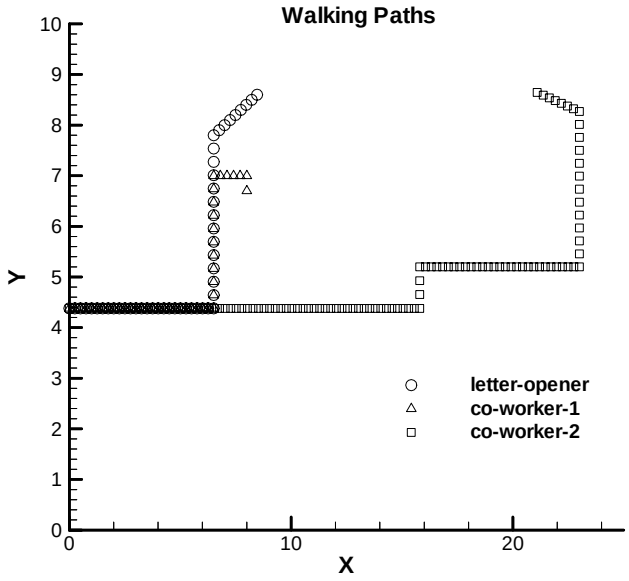

Figure 25: walking paths for LO, CW1 and CW2 for scenarios 1 and 2.

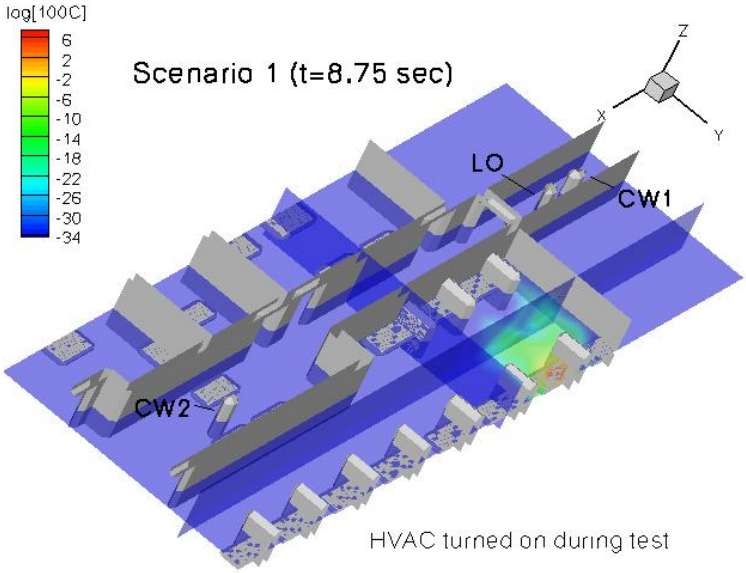

Figure 26: Contours of concentration for Scenario 1a (HVAC is turned on during the test) at *t* = 8.75 sec.

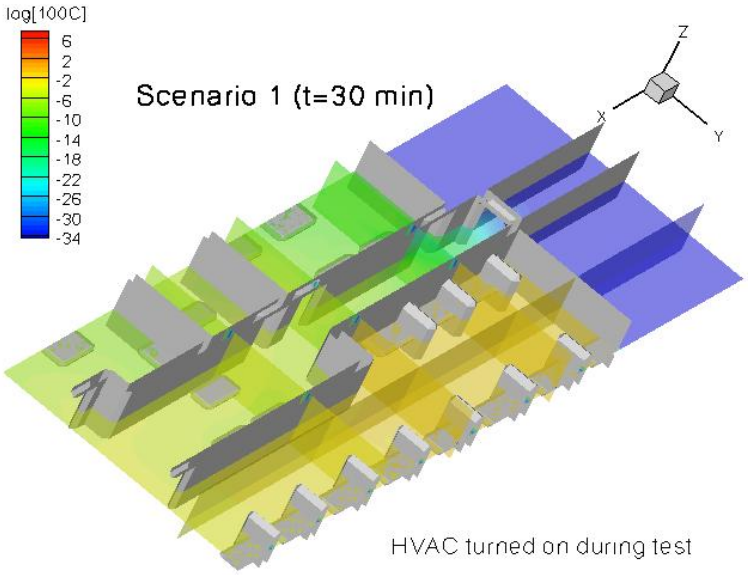

Figure 27: Contours of concentration for Scenario 1a (HVAC is turned on during the test) at *t* = 30 min.

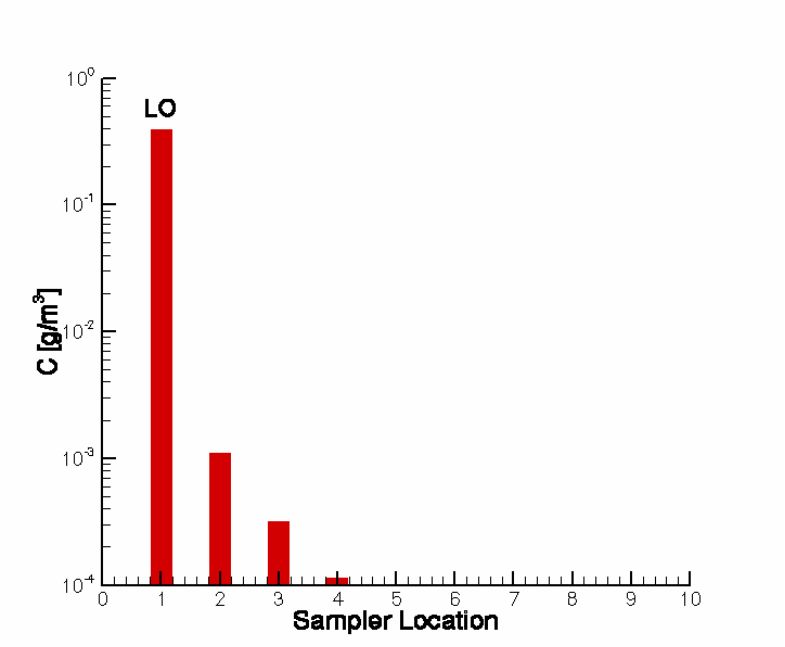

Figure 28: Bar charts of concentration in g m^{-3} at the SKC locations for Scenario 1a (HVAC is turned on during the test).

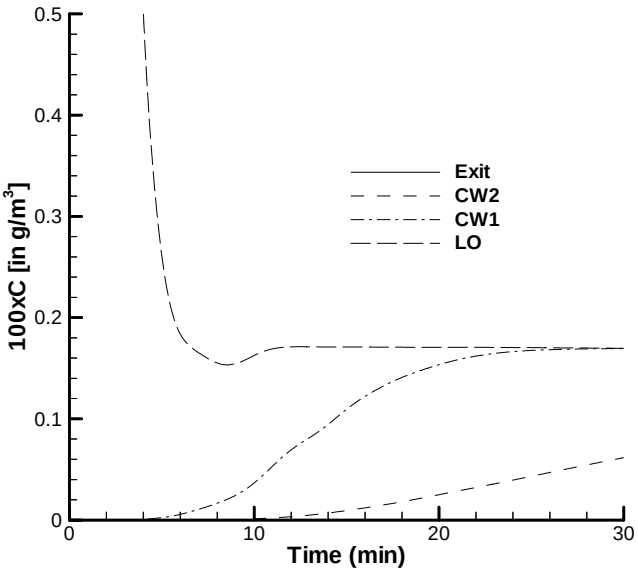

Figure 29: Time histories of concentration in g m^{-3} at the HR locations for Scenario 1a (HVAC is turned on during the test).

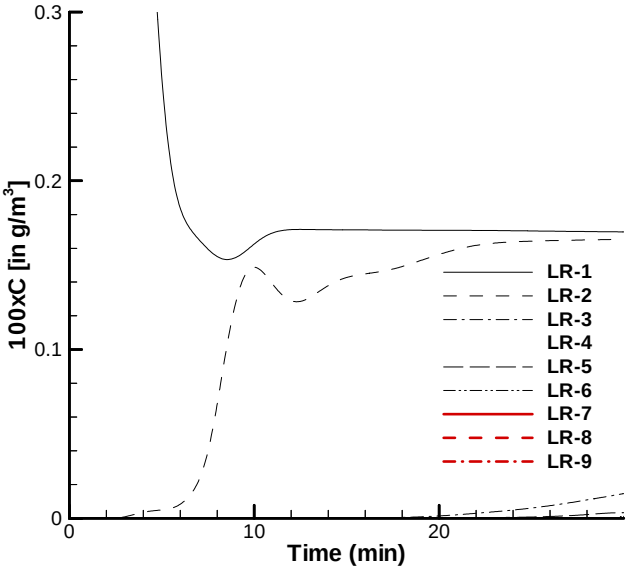

Figure 30: Time histories of concentration in g m^{-3} at the LR locations for Scenario 1a (HVAC is turned on during the test).

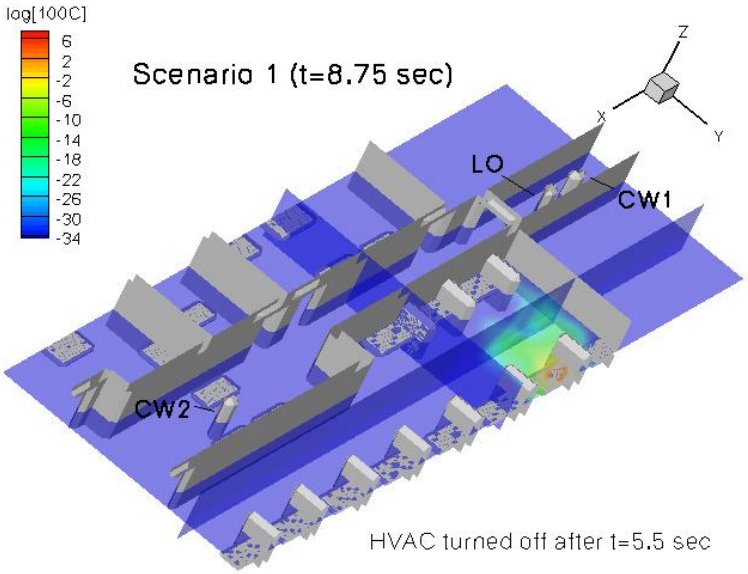

Figure 31: Contours of concentration for Scenario 1b (HVAC is turned off after *t* = 5.5 sec) at *t* = 8.75 sec.

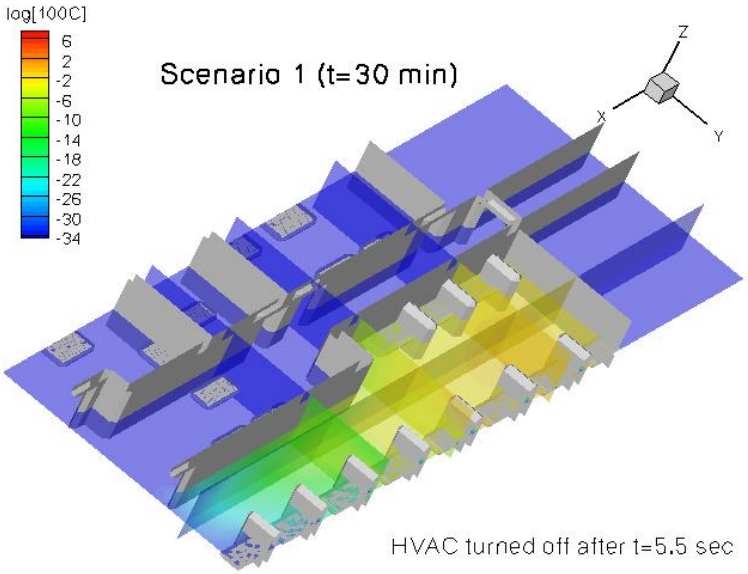

Figure 32: Contours of concentration for Scenario 1b (HVAC is turned off after *t* = 5.5 sec) at *t* = 30 min.

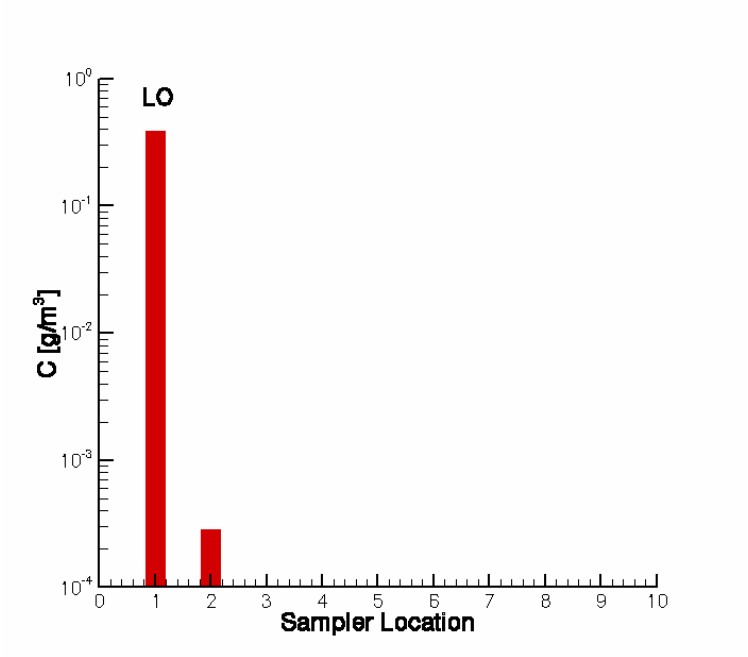

Figure 33: Bar charts of concentration in g m^{-3} at the SKC locations for Scenario 1b (HVAC is turned off after t = 5.5 sec).

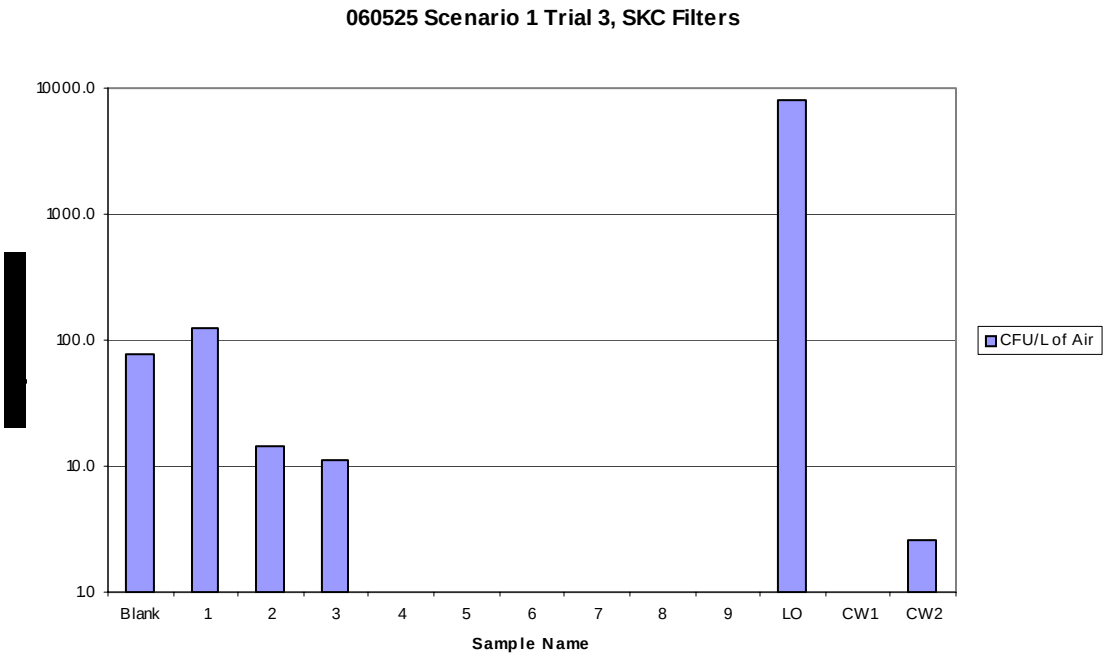

Figure 34: Bar charts of concentration from experiment (Trial 3) in CPU per Liter of Air at the SKC locations for Scenario 1.

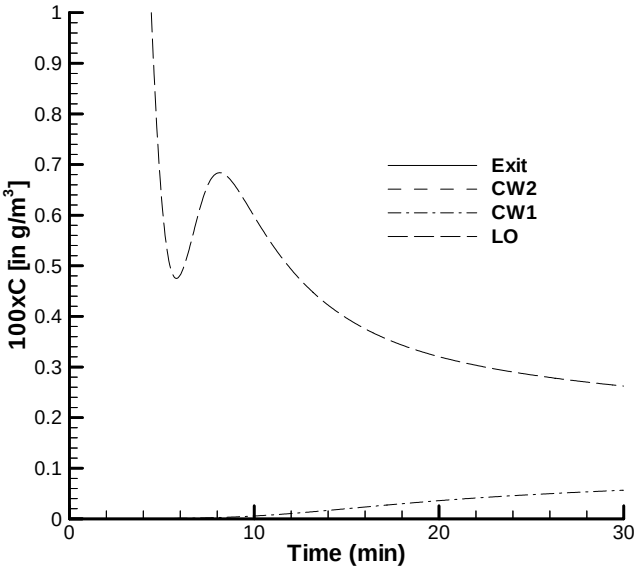

Figure 35: Time histories of concentration in g m^{-3} at the HR locations for Scenario 1b (HVAC is turned off after *t* = 5.5 sec).

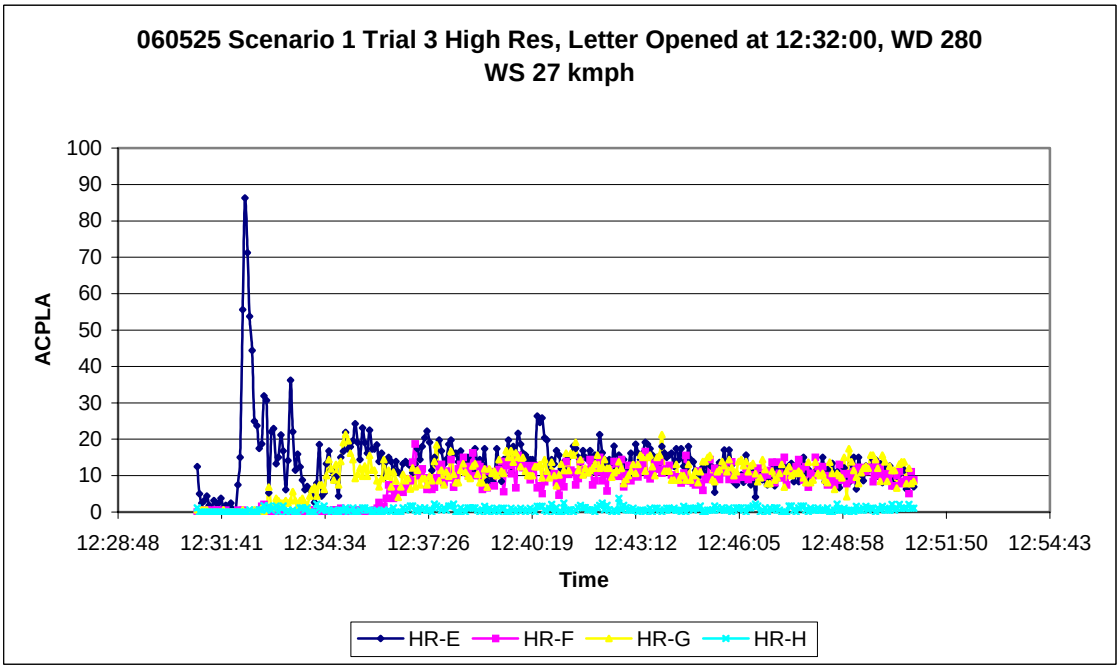

Figure 36: Time histories of concentration in ACPLA from experiment (Trial 3) at the HR locations for Scenario 1.

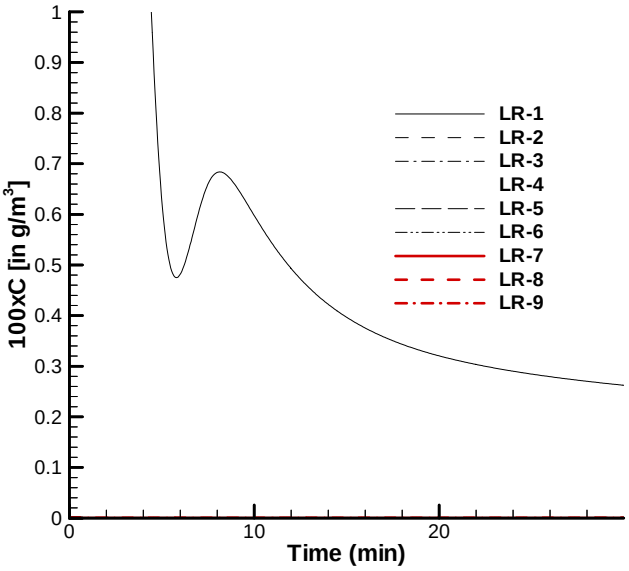

Figure 37: Time histories of concentration in g m^{-3} at the LR locations for Scenario 1b (HVAC is turned off after *t* = 5.5 sec).

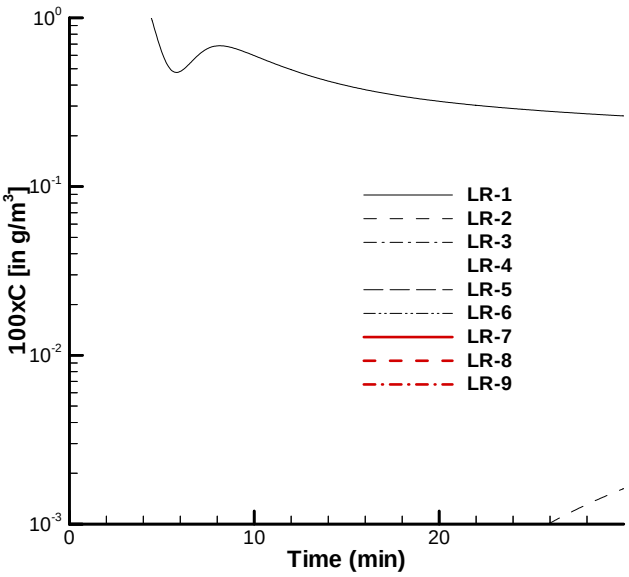

Figure 38: Time histories of concentration in g m^{-3} at the LR locations for Scenario 1b (log scale along *y*-axis).

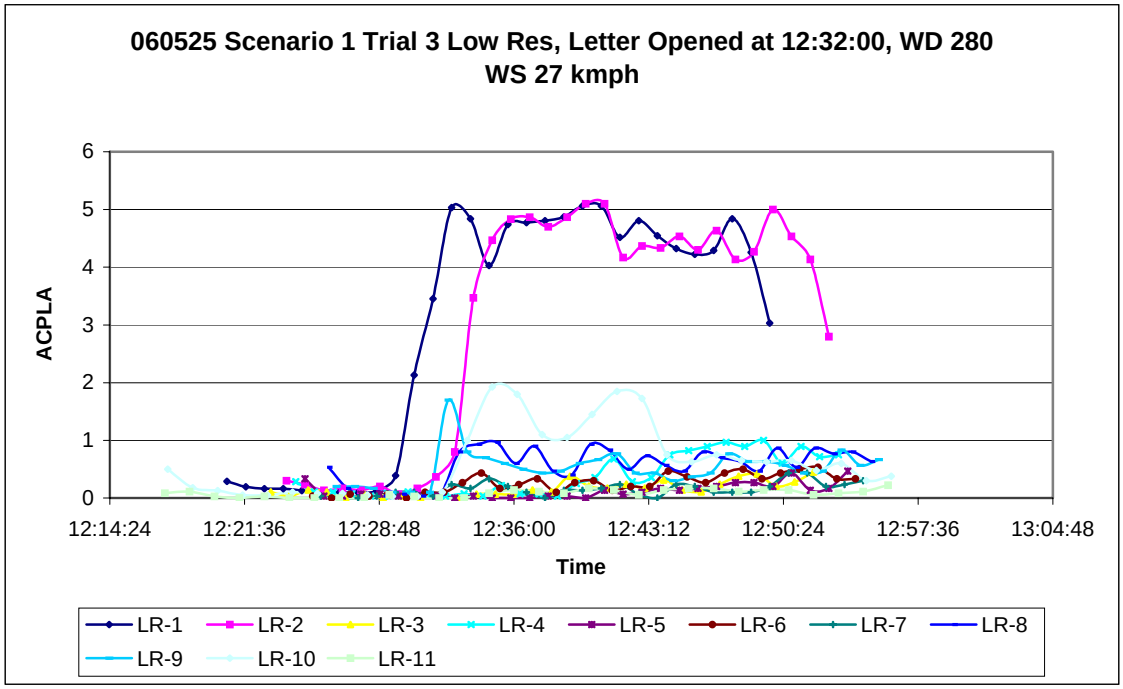

Figure 39: Time histories of concentration in ACPLA from experiment (Trial 3) at the LR locations for Scenario 1.

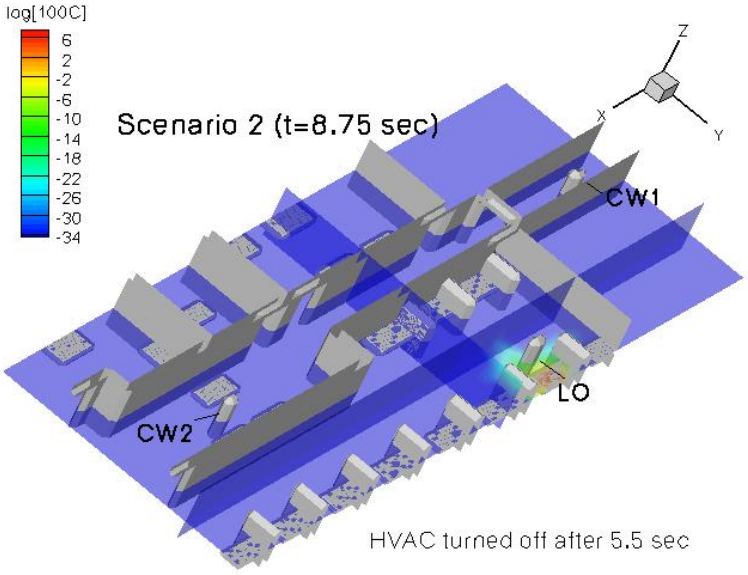

Figure 40: of concentration for Scenario 2 at *t* =8.75 sec.

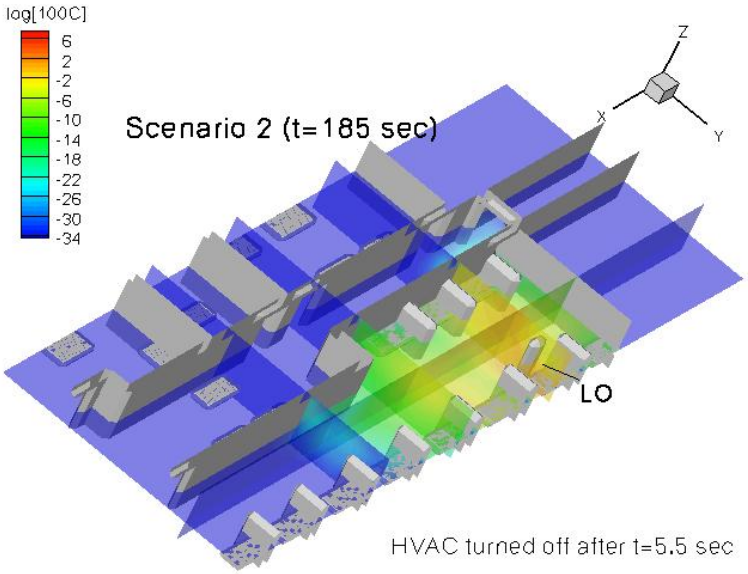

Figure 41: Contours of concentration for Scenario 2 at *t* = 185 sec.

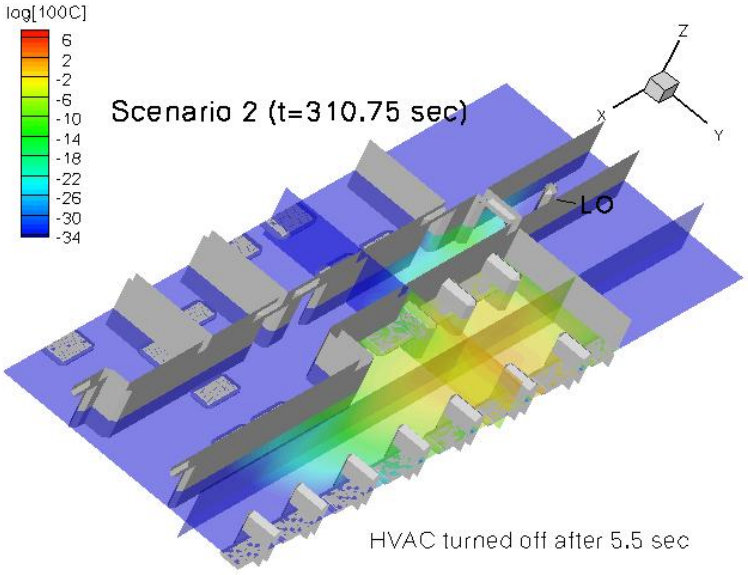

Figure 42: Contours of concentration for Scenario 2 at *t* = 310.75 sec.

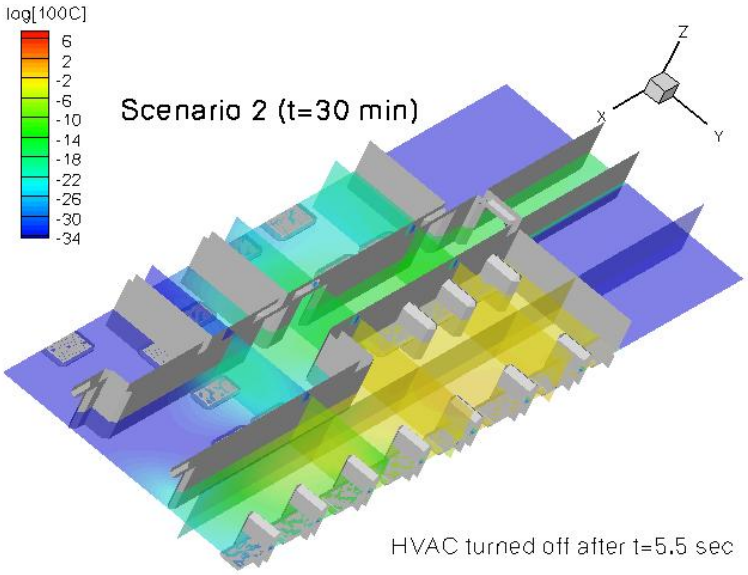

Figure 43: Contours of concentration for Scenario 2 at *t* = 30 min.

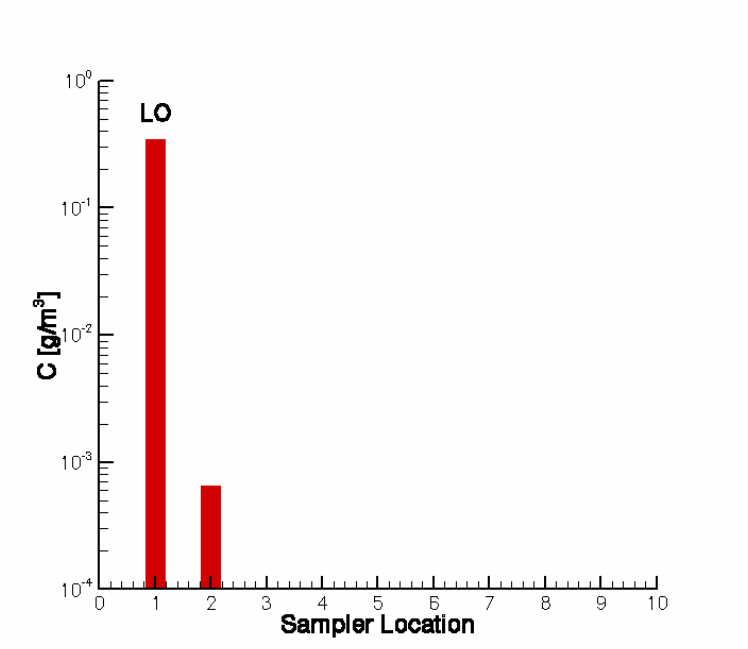

Figure 44: Bar charts of concentration in g m^{-3} at the SKC locations for Scenario 2.

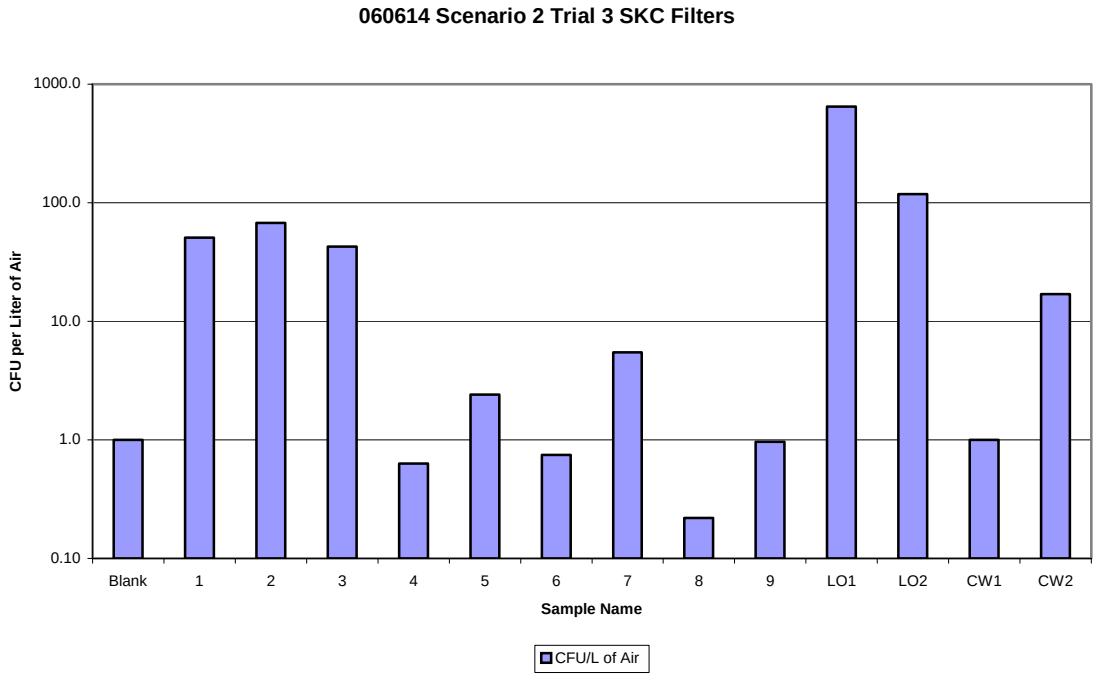

Figure 45: Bar charts of concentration from experiment (Trial 3) in CPU per Liter of Air at the SKC locations for Scenario 2.

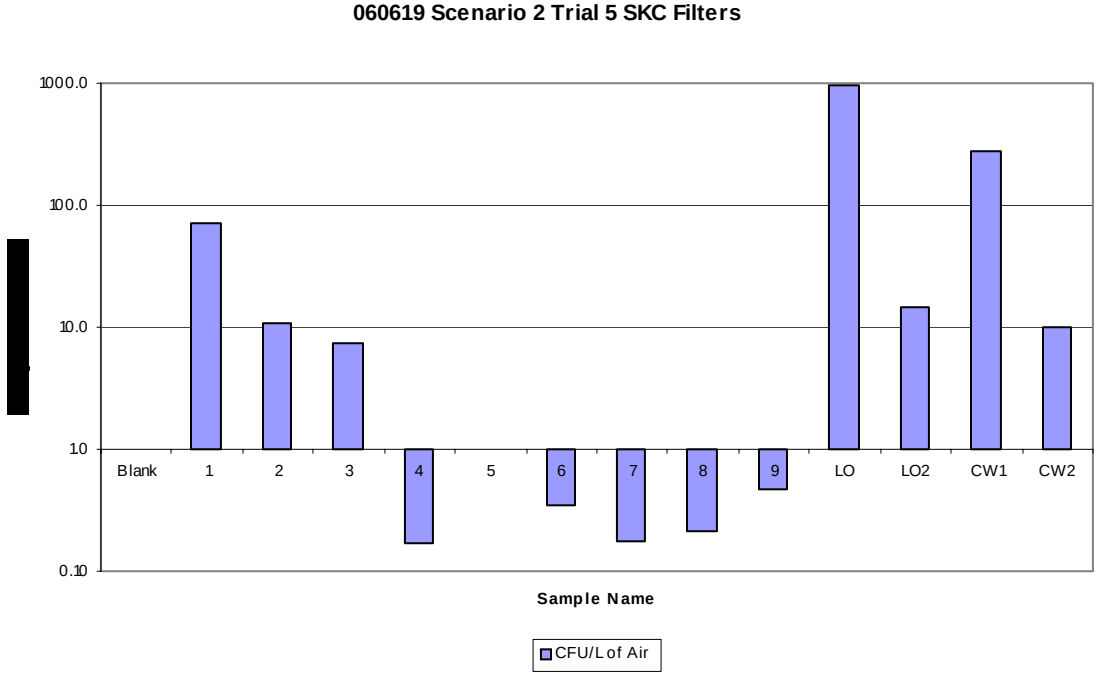

Figure 46: Bar charts of concentration from experiment (Trial 5) in CPU per Liter of Air at SKC locations for Scenario 2.

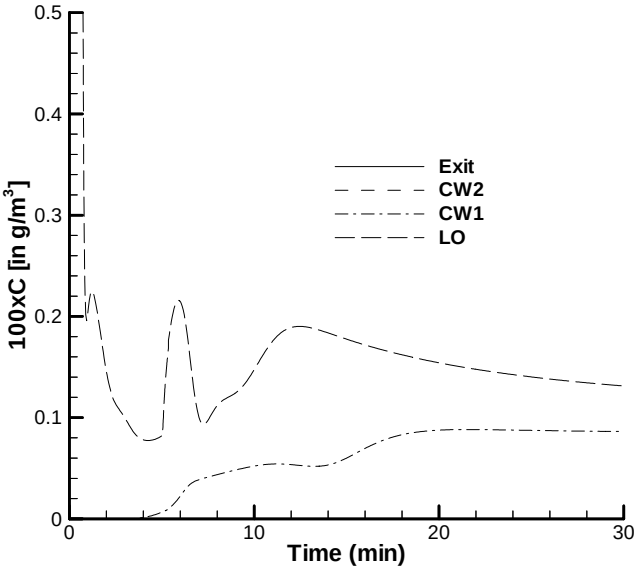

Figure 47: Time histories of concentration in g m^{-3} at the HR locations for Scenario 2 (linear scale along *y*-axis).

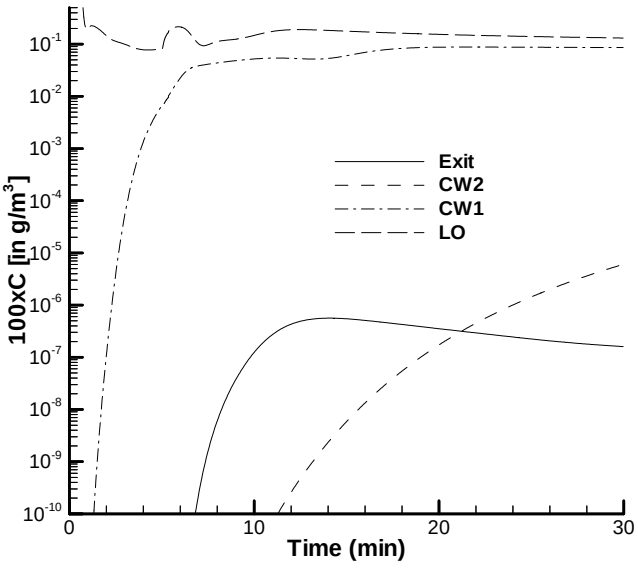

Figure 48: Time histories of concentration in g m^{-3} at the HR locations for Scenario 2 (logarithmic scale along *y*-axis).

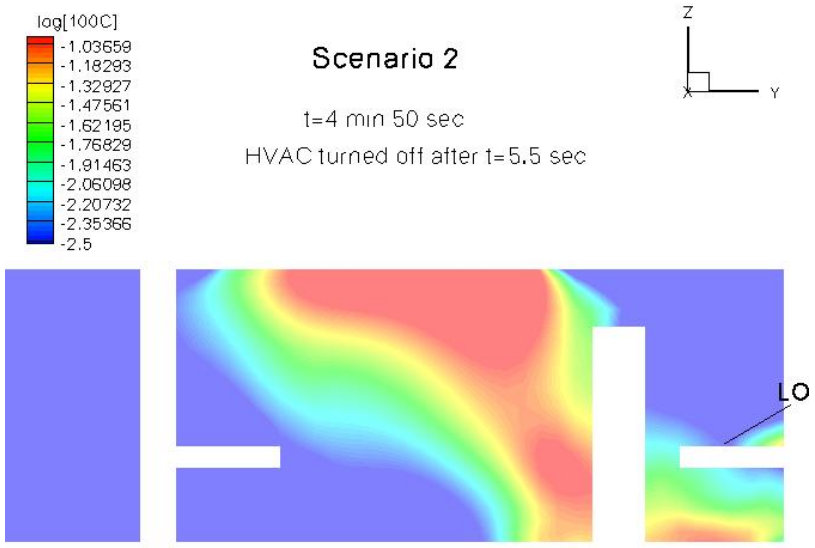

Figure 49: Contours of concentration for Scenario 2 on a vertical *y-z* plane at LO at *t* = 4 min 50 sec.

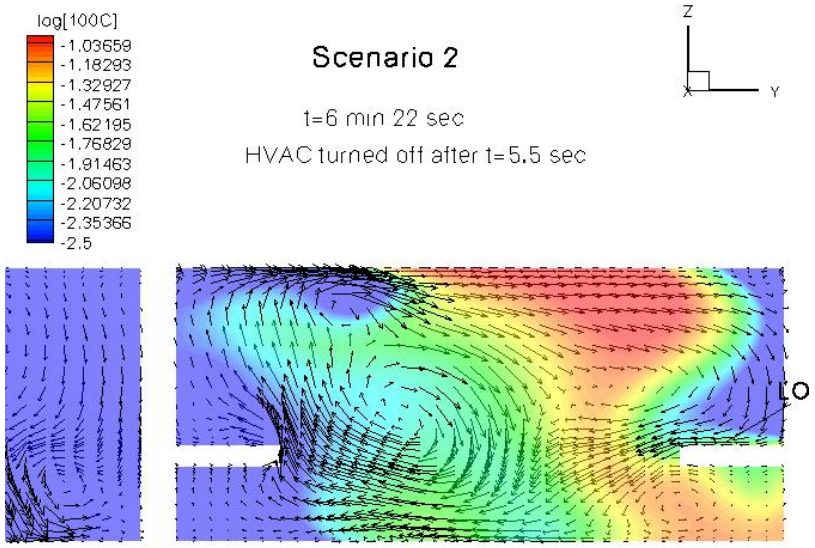

Figure 50: Contours of concentration and velocity vectors for Scenario 2 on a vertical *y-z* plane at LO at *t* = 6 min 22 sec.

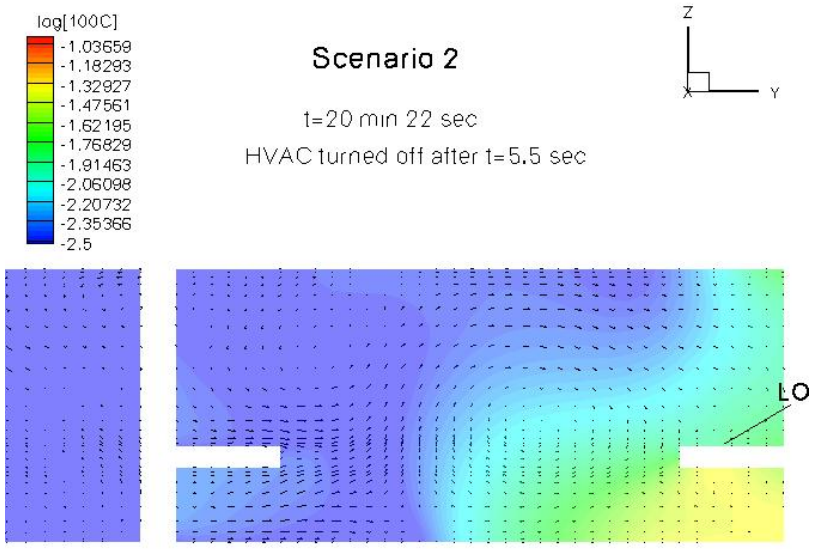

Figure 51: Contours of concentration and velocity vectors for Scenario 2 on a vertical *y-z* plane at LO at *t* = 20 min 22 sec.

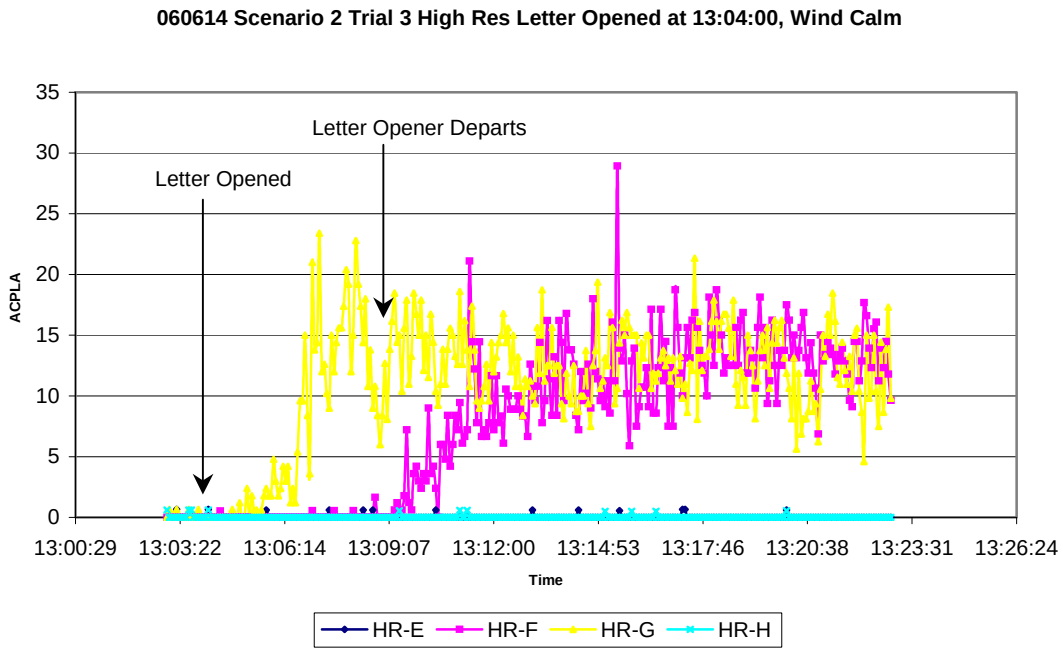

Figure 52: Time histories of concentration in ACPLA from experiment (Trial 3) at the HR locations for Scenario 2.

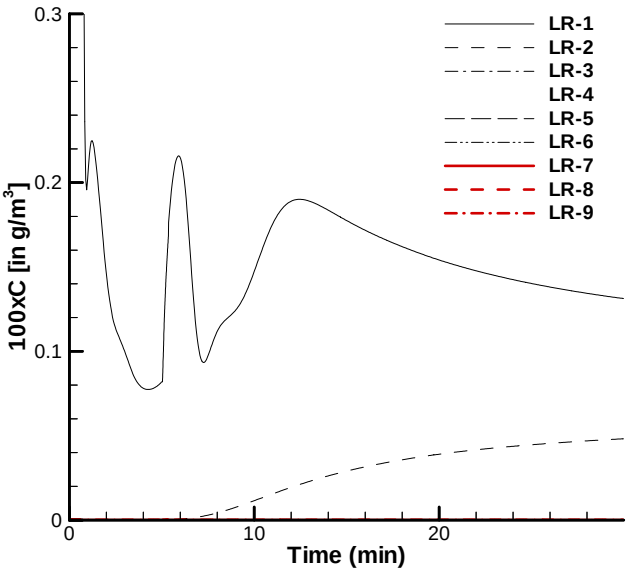

Figure 53: Time histories of concentration in g m^{-3} at the LR locations for Scenario 2 (linear scale along *y*-axis).

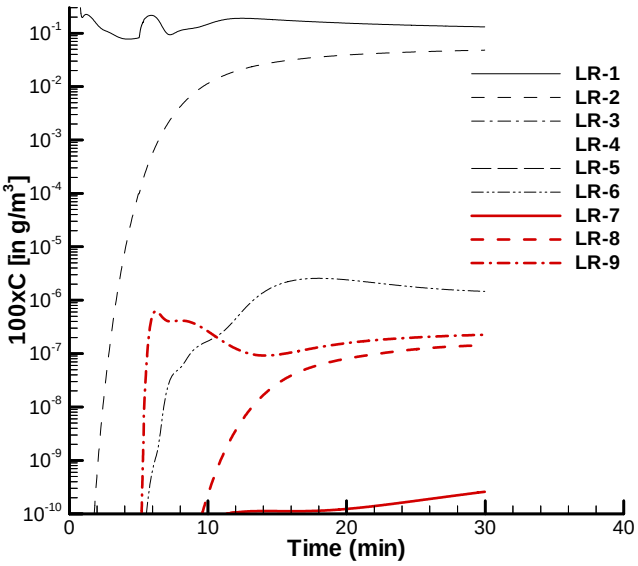

Figure 54: Time histories of concentration in g m^{-3} at the LR locations for Scenario 2 (logarithmic scale along *y*-axis).

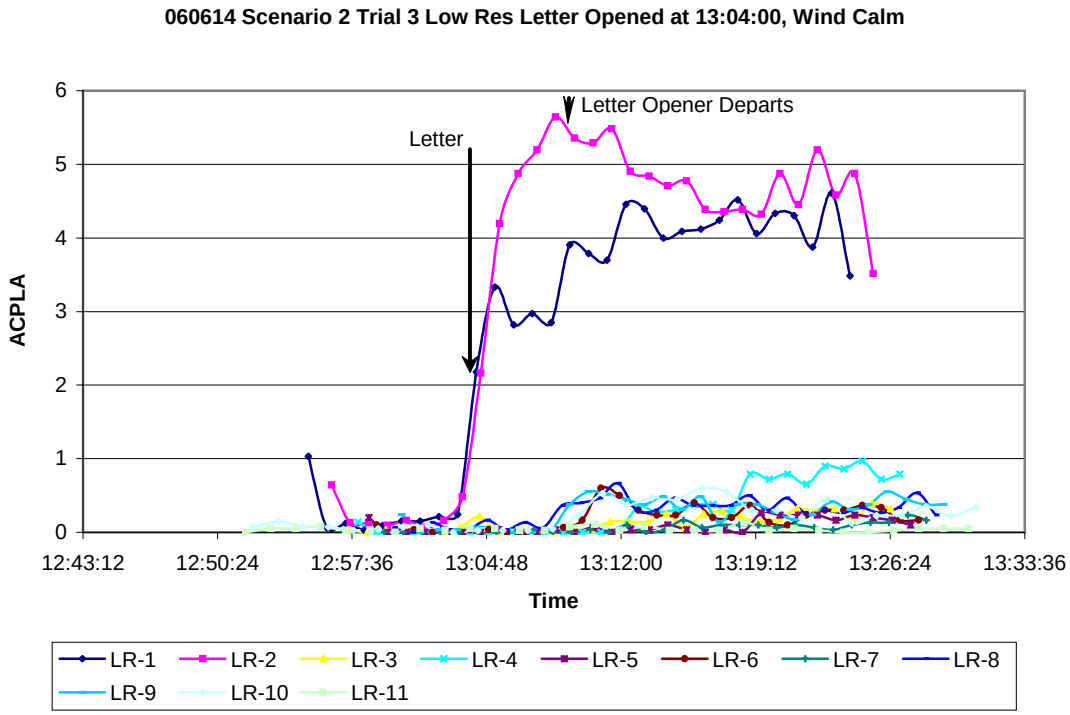

Figure 55: Time histories of concentration in ACPLA from experiment (Trial 3) at the LR locations for Scenario 2.

DOCUMENT CONTROL DATA

(Security classification of title, body of abstract and indexing annotation must be entered when the overall document is classified)

1. ORIGINATOR (the name and address of the organization preparing the document. Organizations for who the document was prepared, e.g. Establishment sponsoring a contractor's report, or tasking agency, are entered in Section 8.)

Waterloo CFD Engineering Consulting Inc.
534 Paradise Crescent
Waterloo, ON N2L 3G1

2. SECURITY CLASSIFICATION (overall security classification of the document, including special warning terms if applicable)

Unclassified

3. TITLE (the complete document title as indicated on the title page. Its classification should be indicated by the appropriate abbreviation (S, C or U) in parentheses after the title).

Prediction of Aerosol Hazard Arising from the Opening of an Anthrax Letter in an Open-Office Environment Using Computational Fluid Dynamics (U)

4. AUTHORS (Last name, first name, middle initial. If military, show rank, e.g. Doe, Maj. John E.)

Lien, F.-S. and Ji, H.

5. DATE OF PUBLICATION (month and year of publication of document)

October 2006

6a. NO. OF PAGES (total containing information, include Annexes, Appendices, etc) 55

6b. NO. OF REFS (total cited in document) 15

7. DESCRIPTIVE NOTES (the category of the document, e.g. technical report, technical note or memorandum. If appropriate, enter the type of report, e.g. interim, progress, summary, annual or final. Give the inclusive dates when a specific reporting period is covered.)

Final Contract Report

8. SPONSORING ACTIVITY (the name of the department project office or laboratory sponsoring the research and development. Include the address.)

Defence R&D Canada – Suffield

9a. PROJECT OR GRANT NO. (If appropriate, the applicable research and development project or grant number under which the document was written. Please specify whether project or grant.)

9b. CONTRACT NO. (If appropriate, the applicable number under which the document was written.)

W7702-05R099

10a. ORIGINATOR'S DOCUMENT NUMBER (the official document number by which the document is identified by the originating activity. This number must be unique to this document.)

DRDC Suffield CR 2006-210

10b. OTHER DOCUMENT NOs. (Any other numbers which may be assigned this document either by the originator or by the sponsor.)

11. DOCUMENT AVAILABILITY (any limitations on further dissemination of the document, other than those imposed by security classification)

(x) Unlimited distribution
( ) Distribution limited to defence departments and defence contractors; further distribution only as approved
( ) Distribution limited to defence departments and Canadian defence contractors; further distribution only as approved
( ) Distribution limited to government departments and agencies; further distribution only as approved
( ) Distribution limited to defence departments; further distribution only as approved
( ) Other (please specify):

12. DOCUMENT ANNOUNCEMENT (any limitation to the bibliographic announcement of this document. This will normally corresponded to the Document Availability (11). However, where further distribution (beyond the audience specified in 11) is possible, a wider announcement audience may be selected).

No limitation on document announcement

13. ABSTRACT (a brief and factual summary of the document. It may also appear elsewhere in the body of the document itself. It is highly desirable that the abstract of classified documents be unclassified. Each paragraph of the abstract shall begin with an indication of the security classification of the information in the paragraph (unless the document itself is unclassified) represented as (S), (C) or (U). It is not necessary to include here abstracts in both official languages unless the text is bilingual).

Early experimental work, conducted at Defence R&D Canada – Suffield, measured and characterized the personal and environmental contamination associated with simulated anthrax-tainted letters under a number of different scenarios in order to obtain a better understanding of the physical and biological processes for detecting, assessing, and formulating potential mitigation strategies for managing the risks associated with opening an anthrax-tainted letter. These preliminary experimental investigations have been extended in the present study to simulate the contamination from anthrax-tainted letters in an Open-Office environment using Computational Fluid Dynamics (CFD). A quantity of 0.1 g of a biological simulant *Bacillus globigii* (BG) for anthrax was released from an opened letter in the experiment. The accuracy of the model for prediction of the spatial distribution of BG spores in the office from the opened letter is assessed qualitatively (and to the extent possible, quantitatively) by detailed comparison with measured BG concentrations obtained under a number of scenarios, some involving people moving within the office. It is hypothesized that the discrepancy between the numerical predictions and experimental measurements of concentration were mainly caused by :

(1) air flow leakage from cracks and crevices in the walls and windows of the building shell;
(2) decoupling between the present CFD simulation and dispersion of BG spores in the Heating, Ventilation, and Air Conditioning (HVAC) system;
(3) the effect of deposition and re-suspension of BG spores not being considered in the present CFD simulations.

Although there is still a scope of further improvement in the present CFD simulation, it should be emphasized here that the advantages of utilization of CFD modeling for assessment and design of mitigation strategies and protocols for defence against anthrax-tainted letters over an experimentally-based approach to the problem are obvious:

(1) substantial reduction of lead times and costs of new designs involving other office configurations;
(2) ability to study scenarios where controlled experiments are difficult or impossible to perform;
(3) practically unlimited level of detail of results such as the flow field in the indoor environment and the concentration field of the dispersing BG spores (or, other contaminants) that are released into this flow field.

14. KEYWORDS, DESCRIPTORS or IDENTIFIERS (technically meaningful terms or short phrases that characterize a document and could be helpful in cataloguing the document. They should be selected so that no security classification is required. Identifies, such as equipment model designation, trade name, military project code name, geographic location may also be included. If possible keywords should be selected from a published thesaurus, e.g. Thesaurus of Engineering and Scientific Terms (TEST) and that thesaurus-identified. If it is not possible to select indexing terms which are Unclassified, the classification of each should be indicated as with the title.)

Computational Fluid Dynamics
Immersed Boundary Methods
Indoor Dispersion
Indoor Air Environment
Anthrax Letter Incidents